Electronic Research Archive

https://www.aimspress.com/journal/era

ERA, 34(7): 4661–4697.
DOI: 10.3934/era.2026206
Received: 02 April 2026
Revised: 03 May 2026
Accepted: 20 May 2026
Published: 29 May 2026

Research article

A new bivariate Kumaraswamy discrete Lindley model: theory and multidisciplinary data analysis

Mahmoud El-Morshedy[1], **Hend S. Shahen**[1,*] **and Mohamed S. Eliwa**[2,3]

[1] Department of Mathematics, College of Science and Humanities in Al-Kharj, Prince Sattam bin Abdulaziz University, Al-Kharj 11942, Saudi Arabia

[2] Department of Statistics and Operations Research, College of Science, Qassim University, Saudi Arabia

[3] Department of Mathematics, Faculty of Science, Mansoura University, Mansoura 35516, Egypt

* **Correspondence:** Email: h.Shahen@psau.edu.sa

Abstract: This study presents the bivariate Kumaraswamy discrete Lindley distribution, developed via a trivariate minimization framework. The model features closed-form formulas for its joint survival, cumulative distribution, and probability mass functions, enabling efficient computer implementation. We analyze the identifiability of the suggested model and the positive dependence structure, deriving the joint probability generating function and conditional expectations. The joint hazard rate function demonstrates considerable distributional flexibility, allowing for monotonic, bathtub, and unimodal shapes. Subsequent to the derivation of maximum likelihood estimators and the Fisher information matrix, we conduct simulation investigations across several sample sizes. The suggested model, when applied to three authentic datasets from the healthcare and manufacturing sectors, demonstrates a better fit than competitive models based on standard statistical selection criteria, confirming its efficacy for modeling count data.

Keywords: statistical model; conditional expectation; simulation; sustainable practices; statistics and numerical data

1. Introduction

In the realm of statistical inference, probability distributions provide the theoretical basis for modeling stochastic phenomena in diverse technical fields. The capacity to derive significant insights and reliable forecasts from empirical data depends heavily on the strategic design of models that accurately reflect the underlying data structure. While theoretical advancements have traditionally focused on univariate cases, the complexity of contemporary datasets demands multivariate

frameworks that can capture interdependent variables. This is especially true for the discrete count data that are common in industrial quality control and biomedical research, where observations such as defect counts or disease incidences necessitate specialized distributions to account for non-standard hazard structures. The Kumaraswamy discrete Lindley (KuDLi) distribution [1] represents a sophisticated response to these modeling challenges, utilizing a three-parameter configuration to provide a highly adaptable framework. Its mathematical foundation is established through the following survival function (SF) and probability mass function (PMF):

$$S_{\text{KuDLi}}(x;\theta,\lambda,q)=\left(1-\left(1-\frac{q^{x+1}\left[1-(x+2)\ln q\right]}{1-\ln q}\right)^{\lambda}\right)^{\theta},\quad x\in\mathbb{N}_0, \tag{1.1}$$

and

$$P_{\text{KuDLi}}(x;\theta,\lambda,q)=\left(1-\left(1-\frac{q^{x}\left[1-(x+1)\ln q\right]}{1-\ln q}\right)^{\lambda}\right)^{\theta}-\left(1-\left(1-\frac{q^{x+1}\left[1-(x+2)\ln q\right]}{1-\ln q}\right)^{\lambda}\right)^{\theta},\quad x\in\mathbb{N}_0, \tag{1.2}$$

where $0<q<1$ and $\lambda,\theta>0$. The KuDLi distribution is characterized by its notable versatility in modeling diverse hazard rate configurations and has demonstrated a highly competitive fit across multiple domains compared with existing baseline models. In contemporary research, modern data acquisition consistently generates multivariate observations where multiple response variables are measured simultaneously within a single experimental unit. Such scenarios are common across various sectors: In industrial manufacturing, multiple defect types often coexist on the same component [2]; in clinical trials, patients frequently display correlated responses across diverse efficacy endpoints [3]; and in environmental monitoring, ecological indicators often exhibit strong spatial or temporal correlations.

Univariate modeling paradigms are inherently insufficient for these contexts, as they fail to account for the dependence structures that govern joint variability, often leading to inefficient inference or erroneous conclusions. However, developing bivariate discrete distributions presents greater theoretical challenges than their continuous counterparts, primarily due to the lack of simple differentiation for density derivation and the combinatorial complexities inherent in discrete support frameworks. While various methodologies such as copula-based approaches and conditional specifications have been proposed to address these challenges, the minimization strategy pioneered by [4] and refined by [5] has proven particularly effective. This approach yields mathematically tractable bivariate families with clear and interpretable dependence structures.

Building on this methodology, several bivariate discrete models have emerged in recent years. These include the discrete phase-type [6], discrete Burr lifetime model [7], generalized exponential [8], Weibull [9], and inverse Weibull [10] distributions. The author in [11] introduced discrete analog for continuous bivariate and multivariate distributions, while the authors of [12] developed a bivariate exponential–geometric model. For a detailed theoretical foundation, see [13, 14]. Furthermore, [15, 16] proposed new construction methodologies utilizing time point process models and the usual stochastic order, respectively. Notwithstanding these theoretical advancements, many deficiencies remain in the literature on bivariate discrete distributions. The current models frequently demonstrate restricted adaptability in concurrently addressing the varied marginal behaviors and intricate dependence structures present in practical applications. Moreover,

numerous proposed distributions do not possess closed-form formulas for essential distributional parameters, thereby constraining their practical applicability. The industrial engineering and healthcare analytics sectors need adaptable yet efficient models that can accurately represent positive correlations in quality control data, patient outcomes, and operational metrics, all while ensuring computational feasibility for large-scale applications. Driven by these pragmatic necessities and theoretical factors, we present the bivariate Kumaraswamy discrete Lindley (BKuDLi) distribution, formulated through the minimization of three independent KuDLi random variables. This unique distributional approach presents numerous strong theoretical and practical benefits:

(i) The distribution provides closed-form equations for joint survival, cumulative distribution, and probability mass functions (PMFs), enabling efficient computation and implementation.
(ii) Both marginal distributions are part of the adaptable KuDLi family, whose members possess the ability to mimic many properties of count data, including differing amounts of dispersion and forms of hazard rates.
(iii) The approach inherently generates positive quadrant dependence, rendering it particularly appropriate for the correlated count data commonly found in industrial and healthcare contexts.
(iv) The joint hazard rate function (HRF) demonstrates significant form flexibility, allowing for monotonic, bathtub, and unimodal structures.
(v) The model's parameters allow for intuitive interpretations, enhancing subject–matter integration and parameter elicitation in practical applications.

The remainder of this paper is organized as follows. Section 2 defines the BKuDLi distribution and elucidates its fundamental probabilistic framework, deriving the joint cumulative distribution function (CDF), joint SF, joint PMF, and joint HRF; it also demonstrates the model's positive dependence characteristics and provides illustrative visualizations. Section 3 examines the key distributional attributes, including the identifiability of the BKuDLi model, the joint probability generating function (JPGF), and conditional distributions and expectancies. In Section 4, the maximum likelihood estimation (MLE) process is detailed, articulating the likelihood function, the score equations, the Fisher information matrix, and the optimization procedures used for parameter estimation. Section 5 presents a simulation study to assess the finite-sample performance of the MLEs. The practical applicability of the proposed model is demonstrated in Section 6 using three real-world datasets from the fields of healthcare and industrial quality control. Finally, Section 7 concludes the paper with a synthesis of the findings and suggestions for future research avenues.

2. Mathematical foundations and visualization of the BKuDLi distribution

Let $U_1 \sim \text{KuDLi}(\theta_1, \lambda, q)$, $U_2 \sim \text{KuDLi}(\theta_2, \lambda, q)$, and $U_3 \sim \text{KuDLi}(\theta_3, \lambda, q)$ be independent random variables. Defining $X_1 = \min\{U_1, U_3\}$ and $X_2 = \min\{U_2, U_3\}$, the bivariate vector $\mathbf{X} = (X_1, X_2)$ is said to follow the BKuDLi distribution with the parameters $\theta_1, \theta_2, \theta_3, \lambda, q$, denoted by $\text{BKuDLi}(\theta_1, \theta_2, \theta_3, \lambda, q)$. The joint SF of $\mathbf{X}$ for $x_1, x_2 \in \mathbb{N}_0$ and $z = \max\{x_1, x_2\}$ is given by

$$S_{\text{BKuDLi}}(x_1, x_2) = \left(1 - \left(1 - \frac{q^{x_1+1}\left[1 - (x_1+2)\ln q\right]}{1 - \ln q}\right)^{\lambda}\right)^{\theta_1} \left(1 - \left(1 - \frac{q^{x_2+1}\left[1 - (x_2+2)\ln q\right]}{1 - \ln q}\right)^{\lambda}\right)^{\theta_2}$$

$$\times\left(1-\left(1-\frac{q^{z+1}\left[1-(z+2)\ln q\right]}{1-\ln q}\right)^{\lambda}\right)^{\theta_3},$$

$$= S_{\text{KuDLi}}(x_1;\theta_1,\lambda,q)\,S_{\text{KuDLi}}(x_2;\theta_2,\lambda,q)\,S_{\text{KuDLi}}(z;\theta_3,\lambda,q),$$

$$= \begin{cases} S_{\text{KuDLi}}(x_1;\theta_1+\theta_3,\lambda,q)\,S_{\text{KuDLi}}(x_2;\theta_2,\lambda,q) & \text{if } x_2 < x_1, \\ S_{\text{KuDLi}}(x_1;\theta_1,\lambda,q)\,S_{\text{KuDLi}}(x_2;\theta_2+\theta_3,\lambda,q) & \text{if } x_1 < x_2, \\ S_{\text{KuDLi}}(x;\theta_1+\theta_2+\theta_3,\lambda,q) & \text{if } x_1 = x_2 = x. \end{cases}$$

The marginal SF of the BKuDLi distribution are obtained as follows:

$$S_{X_i}(x_i;\theta_i,\theta_3,\lambda,q) = P\left[\min(U_i,U_3)\geq x_i\right] = S_{\text{KuDLi}}(x_i;\theta_i+\theta_3,\lambda,q), \quad i=1,2.$$

The joint PMF of the BKuDLi distribution can be expressed as follows:

$$P_{\text{BKuDLi}}(x_1,x_2) = \begin{cases} P_1(x_1,x_2) & \text{if } x_2 < x_1, \\ P_2(x_1,x_2) & \text{if } x_1 < x_2, \\ P_3(x) & \text{if } x_1 = x_2 = x, \end{cases} \tag{2.1}$$

where

$$P_1(x_1,x_2) = \left[\left(1-\left(1-\frac{q^{x_1}\left[1-(x_1+1)\ln q\right]}{1-\ln q}\right)^{\lambda}\right)^{\theta_1+\theta_3} - \left(1-\left(1-\frac{q^{x_1+1}\left[1-(x_1+2)\ln q\right]}{1-\ln q}\right)^{\lambda}\right)^{\theta_1+\theta_3}\right]$$

$$\times\left[\left(1-\left(1-\frac{q^{x_2}\left[1-(x_2+1)\ln q\right]}{1-\ln q}\right)^{\lambda}\right)^{\theta_2} - \left(1-\left(1-\frac{q^{x_2+1}\left[1-(x_2+2)\ln q\right]}{1-\ln q}\right)^{\lambda}\right)^{\theta_2}\right],$$

$$= P_{\text{KuDLi}}(x_1;\theta_1+\theta_3,\lambda,q)\,P_{\text{KuDLi}}(x_2;\theta_2,\lambda,q),$$

$$P_2(x_1,x_2) = \left[\left(1-\left(1-\frac{q^{x_1}\left[1-(x_1+1)\ln q\right]}{1-\ln q}\right)^{\lambda}\right)^{\theta_1} - \left(1-\left(1-\frac{q^{x_1+1}\left[1-(x_1+2)\ln q\right]}{1-\ln q}\right)^{\lambda}\right)^{\theta_1}\right]$$

$$\times\left[\left(1-\left(1-\frac{q^{x_2}\left[1-(x_2+1)\ln q\right]}{1-\ln q}\right)^{\lambda}\right)^{\theta_2+\theta_3} - \left(1-\left(1-\frac{q^{x_2+1}\left[1-(x_2+2)\ln q\right]}{1-\ln q}\right)^{\lambda}\right)^{\theta_2+\theta_3}\right],$$

$$= P_{\text{KuDLi}}(x_1;\theta_1,\lambda,q)\,P_{\text{KuDLi}}(x_2;\theta_2+\theta_3,\lambda,q),$$

and

$$P_3(x,x) = \left(1-\left(1-\frac{q^{x}\left[1-(x+1)\ln q\right]}{1-\ln q}\right)^{\lambda}\right)^{\theta_1} P_{\text{KuDLi}}(x;\theta_2+\theta_3,\lambda,q)$$

$$-\left(1-\left(1-\frac{q^{x+1}\left[1-(x+2)\ln q\right]}{1-\ln q}\right)^{\lambda}\right)^{\theta_1+\theta_3} P_{\text{KuDLi}}(x;\theta_2,\lambda,q).$$

The expressions $P_1(x_1, x_2)$, $P_2(x_1, x_2)$ and $P_3(x, x)$ for $x_1, x_2 \in \mathbb{N}_0$ can be obtained by using the relation

$$P_{X_1,X_2}(x_1, x_2) = S(x_1, x_2) - S(x_1 - 1, x_2) - S(x_1, x_2 - 1) + S(x_1 - 1, x_2 - 1).$$

Figure 1 illustrates the joint PMF of the BKuDLi distribution for various parameter combinations. These visualizations demonstrate the model's capacity to characterize diverse distributional forms, ranging from symmetric configurations to asymmetric patterns exhibiting positive or negative skewness. Notably, the BKuDLi distribution can accommodate heavy-tailed behavior, effectively capturing substantial probability mass in the tail regions. This characteristic is particularly advantageous for modeling extreme count events and identifying outliers in industrial quality control and healthcare diagnostics, where the accurate estimation of tail probabilities is critical for robust risk management and operational planning. The joint CDF of the BKuDLi distribution can be expressed as

$$F_{\text{BKuDLi}}(x_1, x_2) = \begin{cases} F_1(x_1, x_2) & \text{if } x_2 < x_1, \\ F_2(x_1, x_2) & \text{if } x_1 < x_2, \\ F_3(x, x) & \text{if } x_1 = x_2 = x, \end{cases} \tag{2.2}$$

where

$$\begin{aligned} F_1(x_1, x_2) = 1 &- \left(1 - \left(1 - \frac{q^{x_2+1}\left[1 - (x_2 + 2)\ln q\right]}{1 - \ln q}\right)^{\lambda}\right)^{\theta_2+\theta_3} - \left(1 - \left(1 - \frac{q^{x_1+1}\left[1 - (x_1 + 2)\ln q\right]}{1 - \ln q}\right)^{\lambda}\right)^{\theta_1+\theta_3} \\ &\times \left[1 - \left(1 - \left(1 - \frac{q^{x_2+1}\left[1 - (x_2 + 2)\ln q\right]}{1 - \ln q}\right)^{\lambda}\right)^{\theta_2}\right], \end{aligned}$$

$$\begin{aligned} F_2(x_1, x_2) = 1 &- \left(1 - \left(1 - \frac{q^{x_1+1}\left[1 - (x_1 + 2)\ln q\right]}{1 - \ln q}\right)^{\lambda}\right)^{\theta_1+\theta_3} - \left(1 - \left(1 - \frac{q^{x_2+1}\left[1 - (x_2 + 2)\ln q\right]}{1 - \ln q}\right)^{\lambda}\right)^{\theta_2+\theta_3} \\ &\times \left[1 - \left(1 - \left(1 - \frac{q^{x_1+1}\left[1 - (x_1 + 2)\ln q\right]}{1 - \ln q}\right)^{\lambda}\right)^{\theta_1}\right], \end{aligned}$$

and

$$\begin{aligned} F_3(x, x) = 1 &- \left(1 - \left(1 - \frac{q^{x+1}\left[1 - (x + 2)\ln q\right]}{1 - \ln q}\right)^{\lambda}\right)^{\theta_1+\theta_3} - \left(1 - \left(1 - \frac{q^{x+1}\left[1 - (x + 2)\ln q\right]}{1 - \ln q}\right)^{\lambda}\right)^{\theta_2+\theta_3} \\ &+ \left(1 - \left(1 - \frac{q^{x+1}\left[1 - (x + 2)\ln q\right]}{1 - \ln q}\right)^{\lambda}\right)^{\theta_1+\theta_2+\theta_3}. \end{aligned}$$

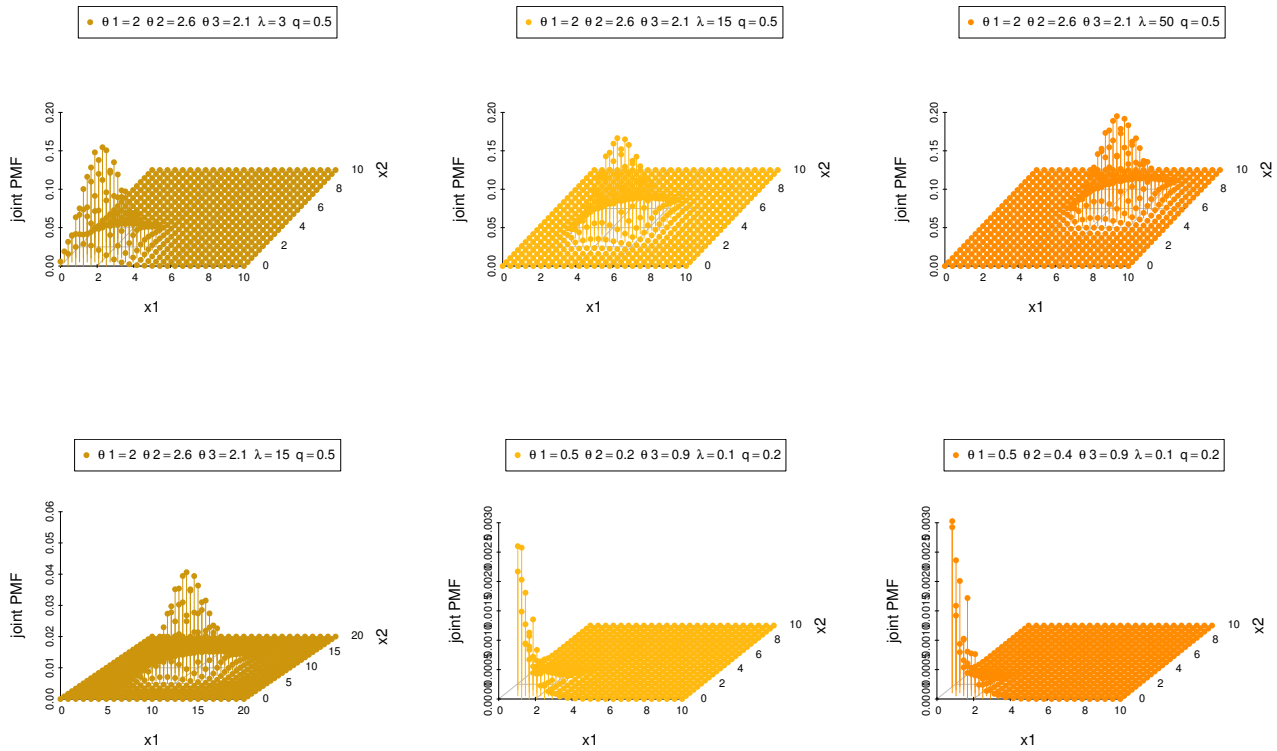

Figure 1. The joint PMF of the BKuDLi distribution for different parameter values.

The joint HRF is defined as

$$h_{\text{BKuDLi}}(x_1, x_2) = \frac{P_{\text{BKuDLi}}(x_1, x_2)}{S_{\text{BKuDLi}}(x_1 - 1, x_2 - 1)},$$

which represents the instantaneous probability of failure at (x_1, x_2) a given survival up to $(x_1 - 1, x_2 - 1)$. The joint reversed HRF is given by

$$Rv_{\text{BKuDLi}}(x_1, x_2) = \frac{P_{\text{BKuDLi}}(x_1, x_2)}{F_{\text{BKuDLi}}(x_1, x_2)},$$

and describes the conditional probability of observing exactly (x_1, x_2) given that the event has already occurred at or before this point. Assume that $(X_{i1}, X_{i2}) \sim \text{BKuDLi}(\theta_{i1}, \theta_{i2}, \theta_{i3}, \lambda, q)$, $i = 1, 2, \ldots, n$, are independent. Define

$$Y_1 = \min\{X_{11}, X_{21}, \ldots, X_{n1}\} \quad \text{and} \quad Y_2 = \min\{X_{12}, X_{22}, \ldots, X_{n2}\}.$$

Then,

$$(Y_1, Y_2) \sim \text{BKuDLi}\left(\sum_{i=1}^{n} \theta_{i1}, \sum_{i=1}^{n} \theta_{i2}, \sum_{i=1}^{n} \theta_{i3}, \lambda, q\right).$$

This closure property under componentwise minimization is particularly useful in reliability engineering, where a system's failure is determined by the earliest component failure among several

independent subsystems. The additive structure of the shape parameters $\theta_{i1}, \theta_{i2}, \theta_{i3}$ provides an interpretable and scalable way to aggregate multiple independent sources of risk. Furthermore, let $X_1 = \min\{U_1, U_3\}$ and $X_2 = \min\{U_2, U_3\}$, where $U_i \sim \text{KuDLi}(\theta_i, \lambda, q)$ for $i = 1, 2, 3$. Then X_1 and X_2 exhibit positive quadrant dependence (PQD). This PQD property arises directly from the minimization-based construction: The common latent variable U_3 induces positive dependence between X_1 and X_2, ensuring that

$$P(X_1 > x_1, X_2 > x_2) \geq P(X_1 > x_1)\, P(X_2 > x_2) \quad \text{for all } (x_1, x_2).$$

This dependence structure is particularly appropriate for modeling industrial quality control scenarios in which failures have shared-cause components, as well as healthcare settings where comorbidities display positive associations. Figures 2 and 3 illustrate the joint SF and joint HRF of the BKuDLi distribution for various parameter values.

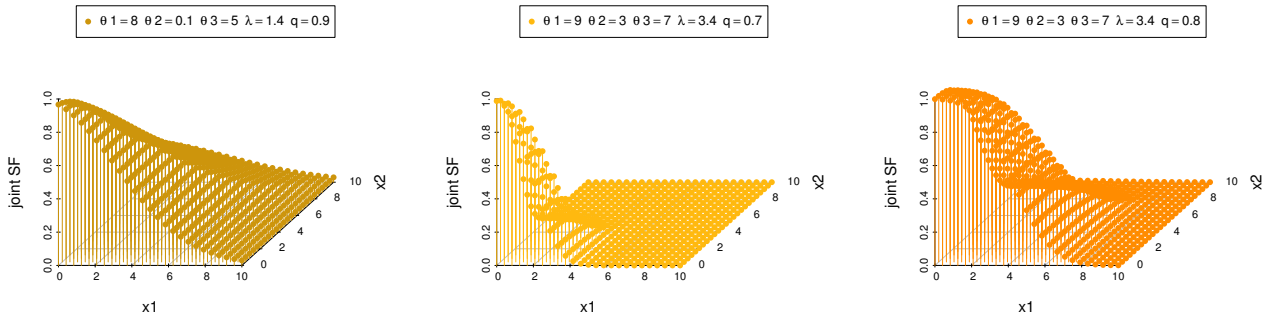

Figure 2. The joint SF of the BKuDLi distribution for different parameter values.

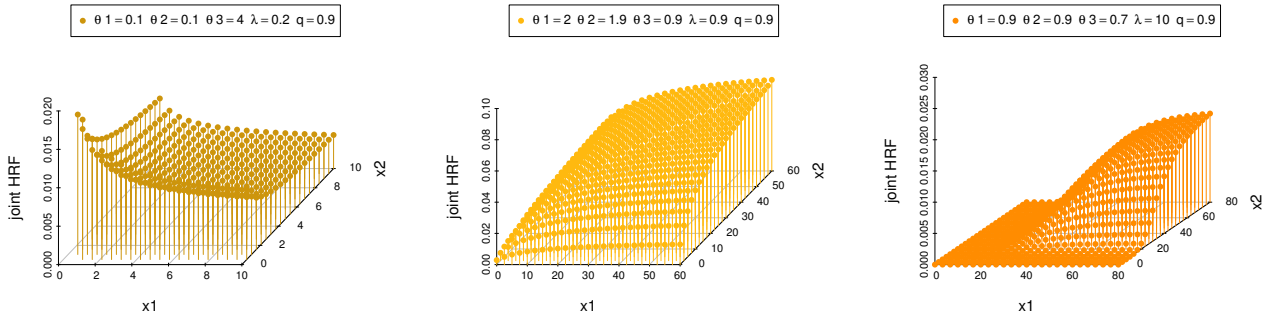

Figure 3. The joint HRF of the BKuDLi distribution for different parameter values.

The visualizations highlight two main features of the BKuDLi model:

(i) The joint SF surfaces are smooth and monotonically decreasing in both dimensions. Their rates of decay are controlled by the parameter vector $(\theta_1, \theta_2, \theta_3, \lambda, q)$, allowing the model to represent

heavy-, moderate-, or light-tailed behavior. Heavy-tailed configurations retain substantial probability mass at large count values, whereas light-tailed configurations produce faster probability decay. The contour shapes also indicate positive dependence between X_1 and X_2, consistent with the theoretically established PQD property. Moreover, changes in θ_1 and θ_2 control the marginal behavior, while θ_3 governing the shared component, enabling the model to capture asymmetric and heterogeneous bivariate count structures.

(ii) The joint HRF surfaces exhibit a wide range of risk patterns under different parameter settings. Some configurations show increasing hazard rates, representing cumulative deterioration or growing risk, while others display bathtub-shaped behavior, reflecting early adaptation followed by wear-out. Nearly constant hazard surfaces may also occur, suggesting approximately memoryless count processes. The parameters λ and q mainly regulate the curvature and rate of change of the hazard surface, whereas the θ parameters determine the relative marginal and common-component effects. Peaks and ridges in the hazard surfaces identify high-risk combinations of (x_1, x_2), which are useful for inspection planning, quality control, and clinical monitoring.

Overall, Figures 2 and 3 provide complementary insights into the distributional behavior of the BKuDLi model. The SF is useful for assessing tail probabilities and extreme-event risk, whereas the HRF describes the dynamic failure or occurrence mechanism. Together, these visualizations confirm the flexibility of the BKuDLi distribution for modeling dependent bivariate count data in industrial reliability, quality control, and healthcare applications.

3. Distributional properties

3.1. Identifiability of the BKuDLi model

The identifiability of the BKuDLi distribution follows from the structural decomposition of its joint PMF and the identifiability of the baseline KuDLi distribution. Let $\boldsymbol{\psi} = (\theta_1, \theta_2, \theta_3, \lambda, q) \in \Omega = \mathbb{R}_+^3 \times \mathbb{R}_+ \times (0, 1)$. The model is identifiable if

$$P_{\text{BKuDLi}}(x_1, x_2; \boldsymbol{\psi}) = P_{\text{BKuDLi}}(x_1, x_2; \boldsymbol{\psi}^*) \ \forall (x_1, x_2) \quad \Rightarrow \quad \boldsymbol{\psi} = \boldsymbol{\psi}^*.$$

From the off-diagonal regions of the joint PMF, we have

$$P_1(x_1, x_2) = P_{\text{KuDLi}}(x_1; \theta_1 + \theta_3, \lambda, q)\, P_{\text{KuDLi}}(x_2; \theta_2, \lambda, q), \quad x_2 < x_1,$$

$$P_2(x_1, x_2) = P_{\text{KuDLi}}(x_1; \theta_1, \lambda, q)\, P_{\text{KuDLi}}(x_2; \theta_2 + \theta_3, \lambda, q), \quad x_1 < x_2,$$

we observe that the quantities θ_1, θ_2, $\theta_1 + \theta_3$, and $\theta_2 + \theta_3$ are separately identifiable through distinct marginal components. Since the KuDLi distribution is identifiable in (θ, λ, q), the equalities of the marginal PMFs imply

$$\theta_1 = \theta_1^*, \quad \theta_2 = \theta_2^*, \quad \theta_1 + \theta_3 = \theta_1^* + \theta_3^*, \quad \theta_2 + \theta_3 = \theta_2^* + \theta_3^*,$$

which yields uniquely

$$\theta_3 = (\theta_1 + \theta_3) - \theta_1.$$

Hence θ_3 is also identifiable. The diagonal component $P_3(x, x)$ further reinforces the identification of θ_3 through the strictly positive probability mass $P(X_1 = X_2) > 0$ when $\theta_3 > 0$, which captures the dependence structure induced by the common latent component. Therefore, the parameter vector $(\theta_1, \theta_2, \theta_3, \lambda, q)$ is globally identifiable on Ω, and no parameter redundancy arises despite the additive appearance of θ_3 in the joint PMF.

3.2. Joint probability generating function of the BKuDLi distribution

The JPGF of the bivariate random vector (X_1, X_2) following the BKuDLi distribution is defined as

$$\mathcal{G}(t_1, t_2) = \mathbb{E}\Big[t_1^{X_1}\, t_2^{X_2}\Big] = \sum_{x_1=0}^{\infty}\sum_{x_2=0}^{\infty} t_1^{x_1}\, t_2^{x_2}\, P_{\text{BKuDLi}}(x_1, x_2), \quad |t_1| \le 1,\ |t_2| \le 1.$$

By decomposing the double sum according to the three regions of the joint PMF, we obtain

$$\mathcal{G}(t_1, t_2) = \mathcal{G}_1(t_1, t_2) + \mathcal{G}_2(t_1, t_2) + \mathcal{G}_3(t_1, t_2),$$

where

$$\begin{aligned}
\mathcal{G}_1(t_1, t_2) &= \sum_{x_1=1}^{\infty}\sum_{x_2=0}^{x_1-1} t_1^{x_1}\, t_2^{x_2}\, P_{\text{KuDLi}}(x_1; \theta_1 + \theta_3, \lambda, q)\, P_{\text{KuDLi}}(x_2; \theta_2, \lambda, q),\\
\mathcal{G}_2(t_1, t_2) &= \sum_{x_2=1}^{\infty}\sum_{x_1=0}^{x_2-1} t_1^{x_1}\, t_2^{x_2}\, P_{\text{KuDLi}}(x_1; \theta_1, \lambda, q)\, P_{\text{KuDLi}}(x_2; \theta_2 + \theta_3, \lambda, q),\\
\mathcal{G}_3(t_1, t_2) &= \sum_{x=0}^{\infty} t_1^{x}\, t_2^{x}\, P_3(x, x).
\end{aligned}$$

For notational convenience, we define the marginal probability generating functions (PGFs) of the KuDLi distribution as

$$G(t; \theta) = \sum_{x=0}^{\infty} t^x\, P_{\text{KuDLi}}(x; \theta, \lambda, q), \quad |t| \le 1,$$

and define the partial generating functions

$$G_{[k]}(t; \theta) = \sum_{x=0}^{k} t^x\, P_{\text{KuDLi}}(x; \theta, \lambda, q), \quad k \in \mathbb{N}_0.$$

Since the summand factorizes over the two regions, we write

$$\begin{aligned}
\mathcal{G}_1(t_1, t_2) &= \sum_{x_1=1}^{\infty} t_1^{x_1}\, P_{\text{KuDLi}}(x_1; \theta_1 + \theta_3, \lambda, q) \sum_{x_2=0}^{x_1-1} t_2^{x_2}\, P_{\text{KuDLi}}(x_2; \theta_2, \lambda, q)\\
&= \sum_{x_1=1}^{\infty} t_1^{x_1}\, P_{\text{KuDLi}}(x_1; \theta_1 + \theta_3, \lambda, q)\, G_{[x_1-1]}(t_2; \theta_2).
\end{aligned}$$

Rewriting $G_{[x_1-1]}(t_2;\theta_2) = G(t_2;\theta_2) - \sum_{x_2=x_1}^{\infty} t_2^{x_2} P_{\text{KuDLi}}(x_2;\theta_2,\lambda,q)$, we obtain

$$\begin{aligned}\mathcal{G}_1(t_1,t_2) &= G(t_2;\theta_2)\sum_{x_1=1}^{\infty} t_1^{x_1} P_{\text{KuDLi}}(x_1;\theta_1+\theta_3,\lambda,q)\\ &\quad - \sum_{x_1=1}^{\infty} t_1^{x_1} P_{\text{KuDLi}}(x_1;\theta_1+\theta_3,\lambda,q)\sum_{x_2=x_1}^{\infty} t_2^{x_2} P_{\text{KuDLi}}(x_2;\theta_2,\lambda,q)\\ &= G(t_2;\theta_2)\left[G(t_1;\theta_1+\theta_3) - P_{\text{KuDLi}}(0;\theta_1+\theta_3,\lambda,q)\right]\\ &\quad - \sum_{x_1=1}^{\infty} t_1^{x_1} P_{\text{KuDLi}}(x_1;\theta_1+\theta_3,\lambda,q)\sum_{x_2=x_1}^{\infty} t_2^{x_2} P_{\text{KuDLi}}(x_2;\theta_2,\lambda,q).\end{aligned}$$

By the same argument applied symmetrically, we obtain

$$\begin{aligned}\mathcal{G}_2(t_1,t_2) &= G(t_1;\theta_1)\left[G(t_2;\theta_2+\theta_3) - P_{\text{KuDLi}}(0;\theta_2+\theta_3,\lambda,q)\right]\\ &\quad - \sum_{x_2=1}^{\infty} t_2^{x_2} P_{\text{KuDLi}}(x_2;\theta_2+\theta_3,\lambda,q)\sum_{x_1=x_2}^{\infty} t_1^{x_1} P_{\text{KuDLi}}(x_1;\theta_1,\lambda,q).\end{aligned}$$

Along the diagonal $x_1 = x_2 = x$, we have $t_1^x t_2^x = (t_1t_2)^x$, so

$$\begin{aligned}\mathcal{G}_3(t_1,t_2) &= \sum_{x=0}^{\infty}(t_1t_2)^x\, P_3(x,x)\\ &= \sum_{x=0}^{\infty}(t_1t_2)^x\left[k(x;\theta_1)\, P_{\text{KuDLi}}(x;\theta_2+\theta_3,\lambda,q) - k(x+1;\theta_1+\theta_3)\, P_{\text{KuDLi}}(x;\theta_2,\lambda,q)\right]\\ &= \sum_{x=0}^{\infty}(t_1t_2)^x\, k(x;\theta_1)\, P_{\text{KuDLi}}(x;\theta_2+\theta_3,\lambda,q)\\ &\quad - \sum_{x=0}^{\infty}(t_1t_2)^x\, k(x+1;\theta_1+\theta_3)\, P_{\text{KuDLi}}(x;\theta_2,\lambda,q),\end{aligned}$$

where $k(x;\theta) = \left(1 - \left(1 - \dfrac{q^x[1-(x+1)\ln q]}{1-\ln q}\right)^{\lambda}\right)^{\theta}$. Combining the three components, the JPGF of the BKuDLi distribution is given by

$$\begin{aligned}\mathcal{G}(t_1,t_2) &= \sum_{i=0}^{\infty}\sum_{j=0}^{i-1} P_{\text{KuDLi}}\,(i;\theta_1+\theta_3,\lambda,q)\, P_{\text{KuDLi}}\,(j;\theta_2,\lambda,q)\, t_1^i t_2^j\\ &\quad + \sum_{i=0}^{\infty}\sum_{j=i+1}^{\infty} P_{\text{KuDLi}}\,(i;\theta_1,\lambda,q)\, P_{\text{KuDLi}}\,(j;\theta_2+\theta_3,\lambda,q)\, t_1^i t_2^j\\ &\quad + \sum_{i=0}^{\infty}\left[k(i;\theta_1)P_{\text{KuDLi}}\,(i;\theta_2+\theta_3,\lambda,q)\; - k(i+1;\theta_1+\theta_3)P_{\text{KuDLi}}\,(i;\theta_2,\lambda,q)\right] t_1^i t_2^i.\end{aligned}$$

Two important special cases follow immediately from the JPGF:

(i) Setting $t_2 = 1$ and $t_1 = 1$ respectively recovers the marginal PGFs:

$$\mathcal{G}(t_1, 1) = G(t_1; \theta_1 + \theta_3), \qquad \mathcal{G}(1, t_2) = G(t_2; \theta_2 + \theta_3),$$

confirming that the marginal distributions of X_1 and X_2 are KuDLi$(\theta_1+\theta_3, \lambda, q)$ and KuDLi$(\theta_2+\theta_3, \lambda, q)$, respectively.
(ii) When $\theta_3 \to 0$, the JPGF factorizes as

$$\mathcal{G}(t_1, t_2)\Big|_{\theta_3=0} = G(t_1; \theta_1)\, G(t_2; \theta_2),$$

confirming that X_1 and X_2 become independent in this limiting case.

3.3. Conditional SF

Let $\mathbf{X} = (X_1, X_2)$ adhere to the BKuDLi distribution. The conditional SF of X_1 given $X_2 = x_2$ is expressed as

$$S_{X_1|X_2=x_2}(x_1|x_2) = \begin{cases} S_1(x_1|x_2) & \text{if } x_2 < x_1, \\ S_2(x_1|x_2) & \text{if } x_1 < x_2, \\ S_3(x_1|x_2) & \text{if } x_1 = x_2 = x, \end{cases} \tag{3.1}$$

where

$$S_1(x_1|x_2) = \frac{\left(1 - \left(1 - \frac{q^{x_1+1}\left[1-(x_1+2)\ln q\right]}{1-\ln q}\right)^{\lambda}\right)^{\theta_1+\theta_3} P_{\text{KuDLi}}(x_2; \theta_2, \lambda, q)}{P_{\text{KuDLi}}(x_2; \theta_2 + \theta_3, \lambda, q)},$$

$$S_2(x_1|x_2) = \left(1 - \left(1 - \frac{q^{x_1+1}\left[1-(x_1+2)\ln q\right]}{1-\ln q}\right)^{\lambda}\right)^{\theta_1},$$

and

$$S_3(x_1|x_2) = \left(1 - \left(1 - \frac{q^{x}\left[1-(x+1)\ln q\right]}{1-\ln q}\right)^{\lambda}\right)^{\theta_1},$$

where $S_{X_1|X_2=x_2}(x_1|x_2) = \frac{P(X_1 \geq x_1, X_2 = x_2)}{P(X_2 = x_2)}$. Similarly, the conditional SF of X_1 given $X_2 \geq x_2$ is given by

$$S_{X_1|X_2\geq x_2}(x_1|x_2) = \begin{cases} \left(1 - \left(1 - \frac{q^{x_1+1}\left[1-(x_1+2)\ln q\right]}{1-\ln q}\right)^{\lambda}\right)^{\theta_1+\theta_3} \left(1 - \left(1 - \frac{q^{x_2+1}\left[1-(x_2+2)\ln q\right]}{1-\ln q}\right)^{\lambda}\right)^{-\theta_3} & \text{if } x_2 < x_1, \\ \left(1 - \left(1 - \frac{q^{x_1+1}\left[1-(x_1+2)\ln q\right]}{1-\ln q}\right)^{\lambda}\right)^{\theta_1} & \text{if } x_1 < x_2, \\ \left(1 - \left(1 - \frac{q^{x+1}\left[1-(x+2)\ln q\right]}{1-\ln q}\right)^{\lambda}\right)^{\theta_1} & \text{if } x_1 = x_2 = x. \end{cases} \tag{3.2}$$

3.4. Conditional PMF

The conditional PMF of X_1 given $X_2 = x_2$ is given by

$$P_{X_1|X_2=x_2}(x_1|x_2) = \begin{cases} P_1(x_1|x_2) & \text{if } x_2 < x_1, \\ P_2(x_1|x_2) & \text{if } x_1 < x_2, \\ P_3(x_1|x_2) & \text{if } x_1 = x_2 = x, \end{cases} \tag{3.3}$$

where

$$P_1(x_1|x_2) = \frac{P_{\text{KuDLi}}(x_1;\theta_1+\theta_3,\lambda,q)\,P_{\text{KuDLi}}(x_2;\theta_2,\lambda,q)}{P_{\text{KuDLi}}(x_2;\theta_2+\theta_3,\lambda,q)},$$

$$P_2(x_1|x_2) = P_{\text{KuDLi}}(x_1;\theta_1,\lambda,q),$$

and

$$P_3(x_1|x_2) = \left(1-\left(1-\frac{q^x\left[1-(x+1)\ln q\right]}{1-\ln q}\right)^{\lambda}\right)^{\theta_1} - \frac{\left(1-\left(1-\frac{q^{x+1}\left[1-(x+2)\ln q\right]}{1-\ln q}\right)^{\lambda}\right)^{\theta_1+\theta_3} P_{\text{KuDLi}}(x;\theta_2,\lambda,q)}{P_{\text{KuDLi}}(x;\theta_2+\theta_3,\lambda,q)}.$$

The conditional expectation of X_1 given $X_2 = x_2$ is obtained as follows:

$$\begin{aligned}\mathbf{E}(X_1|X_2=x_2) = {} & \sum_{x_1=0}^{x_2-1} x_1 P_{\text{KuDLi}}(x_1;\theta_1,\lambda,q) - \frac{x_2\left(1-\left(1-\frac{q^{x_2+1}\left[1-(x_2+2)\ln q\right]}{1-\ln q}\right)^{\lambda}\right)^{\theta_1+\theta_3} P_{\text{KuDLi}}(x_2;\theta_2,\lambda,q)}{P_{\text{KuDLi}}(x_2;\theta_2+\theta_3,\lambda,q)} \\ & + \sum_{x_1=x_2+1}^{\infty} \frac{x_1 P_{\text{KuDLi}}(x_1;\theta_1+\theta_3,\lambda,q)\,P_{\text{KuDLi}}(x_2;\theta_2,\lambda,q)}{P_{\text{KuDLi}}(x_2;\theta_2+\theta_3,\lambda,q)} \\ & + x_2\left(1-\left(1-\frac{q^{x_2}\left[1-(x_2+1)\ln q\right]}{1-\ln q}\right)^{\lambda}\right)^{\theta_1},\end{aligned}$$

where $\mathbf{E}(X_1|X_2=x_2) = \sum_{x_1=0}^{\infty} x_1 P_{X_1|X_2=x_2}(x_1|x_2)$. The conditional PMF of X_2 given $X_1 = x_1$ is given by

$$P_{X_2|X_1=x_1}(x_2|x_1) = \begin{cases} P_1(x_2|x_1) & \text{if } x_2 < x_1, \\ P_2(x_2|x_1) & \text{if } x_1 < x_2, \\ P_3(x_2|x_1) & \text{if } x_1 = x_2 = x, \end{cases} \tag{3.4}$$

where

$$P_1(x_2|x_1) = P_{\text{KuDLi}}(x_2;\theta_2,\lambda,q),$$

$$P_2(x_2|x_1) = \frac{P_{\text{KuDLi}}(x_1;\theta_1,\lambda,q)\,P_{\text{KuDLi}}(x_2;\theta_2+\theta_3,\lambda,q)}{P_{\text{KuDLi}}(x_1;\theta_1+\theta_3,\lambda,q)},$$

and

$$\begin{aligned}P_3(x_2|x_1) = {} & \frac{P_{\text{KuDLi}}(x;\theta_2+\theta_3,\lambda,q)}{P_{\text{KuDLi}}(x;\theta_1+\theta_3,\lambda,q)}\left(1-\left(1-\frac{q^x\left[1-(x+1)\ln q\right]}{1-\ln q}\right)^{\lambda}\right)^{\theta_1} \\ & + \frac{P_{\text{KuDLi}}(x;\theta_2,\lambda,q)}{P_{\text{KuDLi}}(x;\theta_1+\theta_3,\lambda,q)} \times \left(1-\left(1-\frac{q^{x+1}\left[1-(x+2)\ln q\right]}{1-\ln q}\right)^{\lambda}\right)^{\theta_1+\theta_3}.\end{aligned}$$

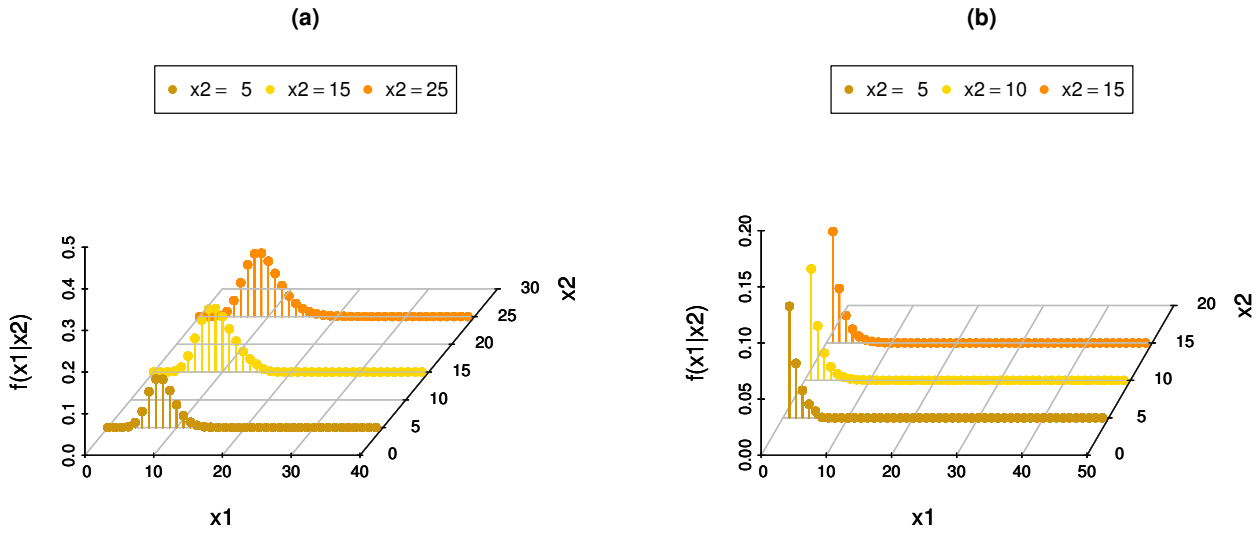

Figure 4. The conditional PMF of X_1 given $X_2 = x_2$ for the BKuDLi distribution.

The conditional PMF of X_1 given $X_2 = x_2$ is depicted in Figure 4 for two different parameter configurations. The left panel depicts $\theta_1 = 2$, $\theta_2 = 2.6$, $\theta_3 = 2.1$, $\lambda = 10$, and $q = 0.7$ with the conditioning values $x_2 = 5$, 15, and 25, whereas the right panel illustrates $\theta_1 = 0.5$, $\theta_2 = 0.2$, $\theta_3 = 0.9$, $\lambda = 0.1$, and $q = 0.2$ with $x_2 = 5$, 10, and 15. In both instances, the probability mass swings toward higher values of X_1 as the conditioning value x_2 increases, showing a positive dependence structure between the variables. The BKuDLi distribution exhibits significant adaptability in fitting diverse geometries of conditional distributions across varying parameter settings.

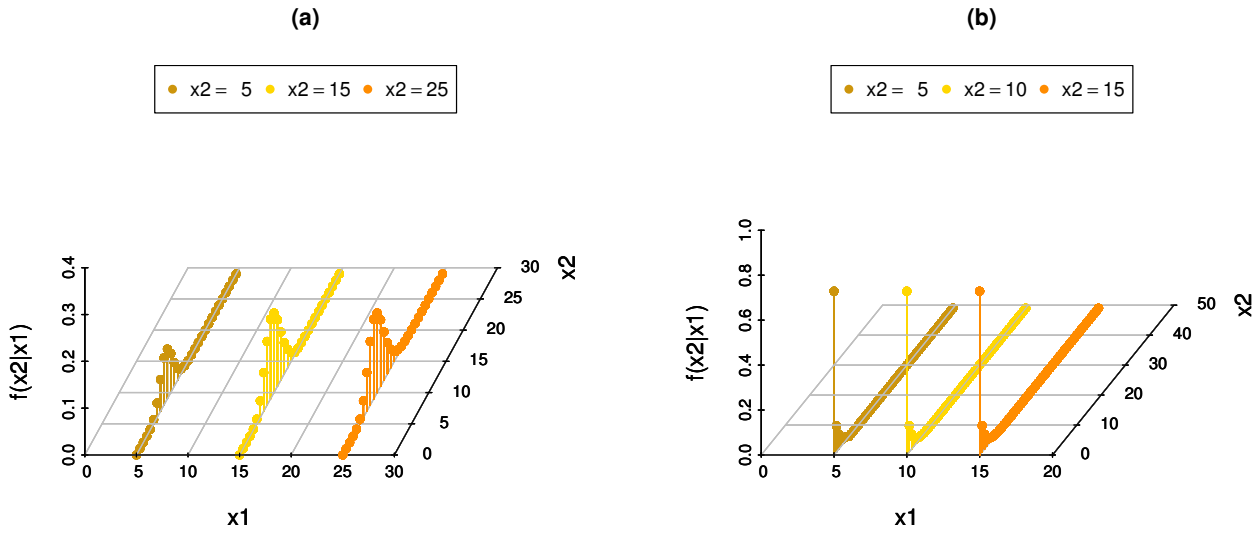

Figure 5. The conditional PMF of X_2 given $X_1 = x_1$ for the BKuDLi distribution.

Figure 5 displays the conditional PMF of X_2 given $X_1 = x_1$ under different parameter specifications. The left panel shows the results for $\theta_1 = 2$, $\theta_2 = 2.6$, $\theta_3 = 2.1$, $\lambda = 15$, $q = 0.7$ with $x_1 = 5, 15, 25$, whereas the right panel presents the case for $\theta_1 = 0.5$, $\theta_2 = 0.4$, $\theta_3 = 0.9$, $\lambda = 0.1$, $q = 0.2$ with $x_1 = 5, 10, 15$. As the conditioning value x_1 increases, the conditional distribution shifts rightward, confirming the positive dependence between X_1 and X_2. The figures demonstrate the suggested distribution's capacity to encapsulate various patterns of conditional behavior across distinct parameter values.

4. Maximum likelihood estimation

This section presents a thorough methodology for estimating the unknown parameters of the BKuDLi distribution via the MLE approach. The MLE method is especially beneficial because of its favorable asymptotic characteristics, such as consistency, asymptotic normalcy, and efficiency under regularity criteria. Let $\mathbf{X} = \{(x_{11}, x_{21}), (x_{12}, x_{22}), \ldots, (x_{1n}, x_{2n})\}$ be a random sample of size n drawn independently from the BKuDLi distribution with the parameter vector $\mathbf{\Theta} = (\theta_1, \theta_2, \theta_3, \lambda, q)^\top$, where $\theta_1, \theta_2, \theta_3 > 0$, $\lambda > 0$, and $0 < q < 1$. To create the likelihood function, we divide the sample space into three mutually exclusive and exhaustive index sets according to the relative ordering of the bivariate observations as follows:

$$I_1 = \{i : x_{1i} > x_{2i}, \quad i = 1, 2, \ldots, n\},$$

$$I_2 = \{i : x_{1i} < x_{2i}, \quad i = 1, 2, \ldots, n\},$$

$$I_3 = \{i : x_{1i} = x_{2i} = x_i, \quad i = 1, 2, \ldots, n\},$$

having equivalent cardinalities $|I_1| = n_1$, $|I_2| = n_2$, and $|I_3| = n_3$, adhering to the condition $n_1+n_2+n_3 = n$. This division is crucial for reflecting the structural dependency present in the bivariate distribution. According to the joint PMF of the BKuDLi distribution and the partition of the sample space, the likelihood function for the parameter vector $\mathbf{\Theta}$ is formulated as the product of three components, each corresponding to a distinct index set as follows:

$$\mathcal{L}(\mathbf{\Theta} \mid \mathbf{X}) = \prod_{i \in I_1} P_1(x_{1i}, x_{2i}; \mathbf{\Theta}) \times \prod_{i \in I_2} P_2(x_{1i}, x_{2i}; \mathbf{\Theta}) \times \prod_{i \in I_3} P_3(x_i, x_i; \mathbf{\Theta}), \tag{4.1}$$

where $P_1(\cdot)$, $P_2(\cdot)$, and $P_3(\cdot)$ denote the probability contributions from each corresponding area of the sample space. The natural logarithm of the likelihood function produces the log-likelihood function, which is more conducive to analytical and numerical optimization.

4.1. Score equations

The log-likelihood function $\ell(\mathbf{\Theta}) = \ln \mathcal{L}(\mathbf{\Theta} \mid \mathbf{X})$ takes the form:

$$\ell(\mathbf{\Theta}) = \sum_{i \in I_1} \ln P_1(x_{1i}, x_{2i}; \mathbf{\Theta}) + \sum_{i \in I_2} \ln P_2(x_{1i}, x_{2i}; \mathbf{\Theta}) + \sum_{i \in I_3} \ln P_3(x_i, x_i; \mathbf{\Theta}). \tag{4.2}$$

To facilitate the derivation of the score equations, we introduce the following compact notation. For any non-negative integer x and parameter λ, define:

$$A(x) = 1 - \frac{q^x\,[1-(x+1)\ln q]}{1-\ln q}, \qquad B(x;\theta,\lambda) = \Big(1 - A(x)^{\lambda}\Big)^{\theta}. \tag{4.3}$$

Therefore, the KuDLi PMF may be written concisely as:

$$P_{\text{KuDLi}}\,(x;\theta,\lambda,q) = B(x;\theta,\lambda) - B(x+1;\theta,\lambda). \tag{4.4}$$

The score vector $\mathbf{S}(\mathbf{\Theta}) = \nabla_{\mathbf{\Theta}}\,\ell(\mathbf{\Theta})$ is obtained by differentiating the log-likelihood with respect to each component of $\mathbf{\Theta} = (\theta_1, \theta_2, \theta_3, \lambda, q)^{\top}$. Setting each score equation to zero yields the following system of maximum likelihood equations:

$$\frac{\partial \ell}{\partial \theta_k} = 0, \quad k = 1,2,3, \qquad \frac{\partial \ell}{\partial \lambda} = 0, \qquad \frac{\partial \ell}{\partial q} = 0. \tag{4.5}$$

Score with respect to θ_1

$$\frac{\partial \ell}{\partial \theta_1} = \sum_{i\in I_1} \frac{\partial}{\partial \theta_1} \ln P_1\,(x_{1i}, x_{2i}) + \sum_{i\in I_2} \frac{\partial}{\partial \theta_1} \ln P_2\,(x_{1i}, x_{2i}) + \sum_{i\in I_3} \frac{\partial}{\partial \theta_1} \ln P_3\,(x_i, x_i) = 0,$$

where the partial derivatives of the individual probability contributions are

$$\begin{aligned}
\frac{\partial}{\partial \theta_1} P_1(x_1,x_2) &= \frac{\partial}{\partial \theta_1}\Big[B(x_1;\theta_1+\theta_3,\lambda) - B(x_1+1;\theta_1+\theta_3,\lambda)\Big] \\
&\quad \times \Big[B(x_2;\theta_2,\lambda) - B(x_2+1;\theta_2,\lambda)\Big], \\
\frac{\partial}{\partial \theta_1} P_2(x_1,x_2) &= \frac{\partial}{\partial \theta_1}\Big[B(x_1;\theta_1,\lambda) - B(x_1+1;\theta_1,\lambda)\Big] \\
&\quad \times \Big[B(x_2;\theta_2+\theta_3,\lambda) - B(x_2+1;\theta_2+\theta_3,\lambda)\Big],
\end{aligned}$$

with the fundamental derivative

$$\frac{\partial}{\partial \theta} B(x;\theta,\lambda) = \Big(1 - A(x)^{\lambda}\Big)^{\theta} \ln\Big(1 - A(x)^{\lambda}\Big).$$

Score with respect to θ_2

$$\frac{\partial \ell}{\partial \theta_2} = \sum_{i\in I_1} \frac{\partial}{\partial \theta_2} \ln P_1\,(x_{1i}, x_{2i}) + \sum_{i\in I_2} \frac{\partial}{\partial \theta_2} \ln P_2\,(x_{1i}, x_{2i}) + \sum_{i\in I_3} \frac{\partial}{\partial \theta_2} \ln P_3\,(x_i, x_i) = 0,$$

where:

$$\begin{aligned}
\frac{\partial}{\partial \theta_2} P_1(x_1,x_2) &= \Big[B(x_1;\theta_1+\theta_3,\lambda) - B(x_1+1;\theta_1+\theta_3,\lambda)\Big] \\
&\quad \times \frac{\partial}{\partial \theta_2}\Big[B(x_2;\theta_2,\lambda) - B(x_2+1;\theta_2,\lambda)\Big], \\
\frac{\partial}{\partial \theta_2} P_2(x_1,x_2) &= \Big[B(x_1;\theta_1,\lambda) - B(x_1+1;\theta_1,\lambda)\Big] \\
&\quad \times \frac{\partial}{\partial \theta_2}\Big[B(x_2;\theta_2+\theta_3,\lambda) - B(x_2+1;\theta_2+\theta_3,\lambda)\Big].
\end{aligned}$$

Score with respect to θ_3

Since θ_3 enters both P_1 and P_2 symmetrically through the combined parameters $(\theta_1 + \theta_3)$ and $(\theta_2 + \theta_3)$, respectively

$$\frac{\partial \ell}{\partial \theta_3} = \sum_{i \in I_1} \frac{\partial}{\partial \theta_3} \ln P_1 (x_{1i}, x_{2i}) + \sum_{i \in I_2} \frac{\partial}{\partial \theta_3} \ln P_2 (x_{1i}, x_{2i}) + \sum_{i \in I_3} \frac{\partial}{\partial \theta_3} \ln P_3 (x_i, x_i) = 0.$$

Score with respect to λ

$$\frac{\partial \ell}{\partial \lambda} = \sum_{i \in I_1} \frac{\partial}{\partial \lambda} \ln P_1 (x_{1i}, x_{2i}) + \sum_{i \in I_2} \frac{\partial}{\partial \lambda} \ln P_2 (x_{1i}, x_{2i}) + \sum_{i \in I_3} \frac{\partial}{\partial \lambda} \ln P_3 (x_i, x_i) = 0,$$

with the following fundamental derivative with respect to λ

$$\frac{\partial}{\partial \lambda} B(x; \theta, \lambda) = -\theta \left(1 - A(x)^{\lambda}\right)^{\theta - 1} A(x)^{\lambda} \ln A(x).$$

Score with respect to q

$$\frac{\partial \ell}{\partial q} = \sum_{i \in I_1} \frac{\partial}{\partial q} \ln P_1 (x_{1i}, x_{2i}) + \sum_{i \in I_2} \frac{\partial}{\partial q} \ln P_2 (x_{1i}, x_{2i}) + \sum_{i \in I_3} \frac{\partial}{\partial q} \ln P_3 (x_i, x_i) = 0,$$

where the derivative of $A(x)$ with respect to q is

$$\frac{\partial}{\partial q} A(x) = \frac{q^{x-1}}{1 - \ln q} \left[x - (x + 1) \ln q - \frac{1 - (x + 1) \ln q}{1 - \ln q} \right],$$

yielding the fundamental building block

$$\frac{\partial}{\partial q} B(x; \theta, \lambda) = -\theta \lambda \left(1 - A(x)^{\lambda}\right)^{\theta - 1} A(x)^{\lambda - 1} \frac{\partial A(x)}{\partial q}.$$

Since the score equations do not admit closed-form solutions, the MLE $\hat{\boldsymbol{\Theta}}$ is obtained numerically by solving the nonlinear system $\mathbf{S}(\boldsymbol{\Theta}) = \mathbf{0}$ using iterative optimization algorithms such as the Newton–Raphson or quasi-Newton methods.

4.2. Fisher information matrix, standard errors, and optimization

The observed Fisher information matrix (FIM) is the 5×5 symmetric negative Hessian of the log-likelihood evaluated at the MLE $\hat{\boldsymbol{\Theta}}$

$$\mathcal{I}\left(\hat{\boldsymbol{\Theta}}\right) = -\mathbf{H}\left(\hat{\boldsymbol{\Theta}}\right) = - \left. \frac{\partial^2 \ell(\boldsymbol{\Theta})}{\partial \boldsymbol{\Theta} \, \partial \boldsymbol{\Theta}^{\top}} \right|_{\boldsymbol{\Theta} = \hat{\boldsymbol{\Theta}}}, \tag{4.6}$$

whose (j, k)-th element is

$$\left[\mathcal{I}\left(\hat{\boldsymbol{\Theta}}\right)\right]_{jk} = - \sum_{i \in \mathcal{S}_1} \frac{\partial^2 \ln P_1}{\partial \Theta_j \, \partial \Theta_k} - \sum_{i \in \mathcal{S}_2} \frac{\partial^2 \ln P_2}{\partial \Theta_j \, \partial \Theta_k} - \sum_{i \in \mathcal{S}_3} \frac{\partial^2 \ln P_3}{\partial \Theta_j \, \partial \Theta_k}, \quad j, k \in \{\theta_1, \theta_2, \theta_3, \lambda, q\}, \tag{4.7}$$

where $\mathcal{S}_1$, $\mathcal{S}_2$, and $\mathcal{S}_3$ are the index sets corresponding to the three ordering regions of the joint PMF. Explicitly, the FIM takes the block form

$$\mathcal{I}\left(\hat{\boldsymbol{\Theta}}\right) = \begin{pmatrix} \mathcal{I}_{\theta_1\theta_1} & \mathcal{I}_{\theta_1\theta_2} & \mathcal{I}_{\theta_1\theta_3} & \mathcal{I}_{\theta_1\lambda} & \mathcal{I}_{\theta_1 q} \\ \mathcal{I}_{\theta_2\theta_1} & \mathcal{I}_{\theta_2\theta_2} & \mathcal{I}_{\theta_2\theta_3} & \mathcal{I}_{\theta_2\lambda} & \mathcal{I}_{\theta_2 q} \\ \mathcal{I}_{\theta_3\theta_1} & \mathcal{I}_{\theta_3\theta_2} & \mathcal{I}_{\theta_3\theta_3} & \mathcal{I}_{\theta_3\lambda} & \mathcal{I}_{\theta_3 q} \\ \mathcal{I}_{\lambda\theta_1} & \mathcal{I}_{\lambda\theta_2} & \mathcal{I}_{\lambda\theta_3} & \mathcal{I}_{\lambda\lambda} & \mathcal{I}_{\lambda q} \\ \mathcal{I}_{q\theta_1} & \mathcal{I}_{q\theta_2} & \mathcal{I}_{q\theta_3} & \mathcal{I}_{q\lambda} & \mathcal{I}_{qq} \end{pmatrix}. \tag{4.8}$$

The key second-order derivatives required to populate the FIM are obtained from the building block $B(x;\theta,\lambda) = \left(1 - A(x)^{\lambda}\right)^{\theta}$, where $A(x) = 1 - \frac{q^x[1-(x+1)\ln q]}{1-\ln q}$, and read

$$\begin{aligned} \frac{\partial^2 B}{\partial\theta^2} &= \left(1 - A(x)^{\lambda}\right)^{\theta}\left[\ln\left(1 - A(x)^{\lambda}\right)\right]^2, \\ \frac{\partial^2 B}{\partial\theta\,\partial\lambda} &= -\left(1 - A(x)^{\lambda}\right)^{\theta-1} A(x)^{\lambda}\ln A(x)\left[1 + \theta\ln\left(1 - A(x)^{\lambda}\right)\right], \\ \frac{\partial^2 B}{\partial\lambda^2} &= \theta\left(1 - A(x)^{\lambda}\right)^{\theta-2} A(x)^{\lambda}[\ln A(x)]^2\left[(\theta-1)A(x)^{\lambda} - \left(1 - A(x)^{\lambda}\right)\right]. \end{aligned}$$

Under standard regularity conditions, the expected and observed Fisher information matrices satisfy

$$\mathbb{E}\left[\mathcal{I}\left(\hat{\boldsymbol{\Theta}}\right)\right] = -\mathbb{E}\left[\nabla^2\ell(\boldsymbol{\Theta})\right] = \mathbb{E}[\mathbf{S}(\boldsymbol{\Theta})\,\mathbf{S}(\boldsymbol{\Theta})^{\top}], \tag{4.9}$$

and the inverse of the observed FIM yields the following asymptotic variance–covariance matrix of the MLEs,

$$\boldsymbol{\Sigma}\left(\hat{\boldsymbol{\Theta}}\right) = \mathcal{I}^{-1}\left(\hat{\boldsymbol{\Theta}}\right) = \begin{pmatrix} \widehat{\mathrm{Var}}(\hat{\theta}_1) & \widehat{\mathrm{Cov}}(\hat{\theta}_1,\hat{\theta}_2) & \cdots & \widehat{\mathrm{Cov}}(\hat{\theta}_1,\hat{q}) \\ \widehat{\mathrm{Cov}}(\hat{\theta}_2,\hat{\theta}_1) & \widehat{\mathrm{Var}}(\hat{\theta}_2) & \cdots & \widehat{\mathrm{Cov}}(\hat{\theta}_2,\hat{q}) \\ \vdots & \vdots & \ddots & \vdots \\ \widehat{\mathrm{Cov}}(\hat{q},\hat{\theta}_1) & \widehat{\mathrm{Cov}}(\hat{q},\hat{\theta}_2) & \cdots & \widehat{\mathrm{Var}}(\hat{q}) \end{pmatrix}, \tag{4.10}$$

provided $\mathcal{I}(\hat{\boldsymbol{\Theta}})$ is positive definite, which is verified numerically at the reported MLE via the Cholesky factorization of $\mathcal{I}(\hat{\boldsymbol{\Theta}})$. By the asymptotic normality of the MLE, we have

$$\sqrt{n}\left(\hat{\boldsymbol{\Theta}} - \boldsymbol{\Theta}_0\right) \xrightarrow{\mathcal{D}} \mathcal{N}_5\left(\mathbf{0},\, \mathcal{I}^{-1}(\boldsymbol{\Theta}_0)\right) \quad \text{as } n \to \infty, \tag{4.11}$$

where $\boldsymbol{\Theta}_0$ is the true parameter vector, such that each individual MLE satisfies

$$\hat{\Theta}_k \overset{\text{approx}}{\sim} \mathcal{N}\left(\Theta_k,\, \left[\boldsymbol{\Sigma}\left(\hat{\boldsymbol{\Theta}}\right)\right]_{kk}\right), \quad k = 1,2,3,4,5. \tag{4.12}$$

The asymptotic standard error of $\hat{\Theta}_k$ is

$$\widehat{\mathrm{SE}}\left(\hat{\Theta}_k\right) = \sqrt{\left[\mathcal{I}^{-1}\left(\hat{\boldsymbol{\Theta}}\right)\right]_{kk}}, \tag{4.13}$$

explicitly yielding

$$\widehat{\mathrm{SE}}(\hat{\theta}_1) = \sqrt{\boldsymbol{\Sigma}_{11}}, \quad \widehat{\mathrm{SE}}(\hat{\theta}_2) = \sqrt{\boldsymbol{\Sigma}_{22}}, \quad \widehat{\mathrm{SE}}(\hat{\theta}_3) = \sqrt{\boldsymbol{\Sigma}_{33}}, \quad \widehat{\mathrm{SE}}(\hat{\lambda}) = \sqrt{\boldsymbol{\Sigma}_{44}}, \quad \widehat{\mathrm{SE}}(\hat{q}) = \sqrt{\boldsymbol{\Sigma}_{55}},$$

and the two-sided 95% asymptotic confidence interval for each Θ_k is

$$\mathrm{CI}_{95\%}(\Theta_k) = \left[\hat{\Theta}_k - 1.96 \cdot \widehat{\mathrm{SE}}\left(\hat{\Theta}_k\right), \quad \hat{\Theta}_k + 1.96 \cdot \widehat{\mathrm{SE}}\left(\hat{\Theta}_k\right)\right]. \tag{4.14}$$

The geometry of the likelihood surface is characterized by the spectral properties of $\mathcal{I}(\hat{\boldsymbol{\Theta}})$. Let $\lambda_1 \geq \lambda_2 \geq \cdots \geq \lambda_5 > 0$ denote its ordered eigenvalues. The curvature of the log-likelihood surface along the k-th eigenvector $\mathbf{v}_k$ satisfies

$$\ell\left(\hat{\boldsymbol{\Theta}} + \epsilon\, \mathbf{v}_k\right) \approx \ell\left(\hat{\boldsymbol{\Theta}}\right) - \frac{\epsilon^2}{2}\lambda_k, \quad \epsilon \to 0, \tag{4.15}$$

so that directions with $\lambda_k \approx 0$ signal flat ridges and potential numerical instability. The overall conditioning of the likelihood surface is measured by the condition number

$$\kappa\left(\mathcal{I}(\hat{\boldsymbol{\Theta}})\right) = \frac{\lambda_{\max}}{\lambda_{\min}}, \tag{4.16}$$

where $\kappa \approx 1$ indicates a well-conditioned surface with a unique, stable maximum, and $\kappa \gg 1$ signals ill-conditioning and heightened sensitivity to the initial values. To safeguard against convergence to local optima arising from the piecewise nonlinear structure of $\ell(\boldsymbol{\Theta})$, the optimization is performed using a hybrid strategy that combines a global stochastic search over $M = 500$ independent random starting points as follows:

$$\boldsymbol{\Theta}_0^{(m)} \sim \mathrm{Uniform}(\Omega_0), \quad \Omega_0 = (0,5)^3 \times (0,5) \times (0.01, 0.99), \quad m = 1, \ldots, M, \tag{4.17}$$

with a local quasi-Newton refinement applied to the top K candidate solutions ranked by their log-likelihood values, yielding the final estimate

$$\hat{\boldsymbol{\Theta}} = \underset{m=1,\ldots,K}{\arg\max}\ \ell\left(\hat{\boldsymbol{\Theta}}^{(m)}\right). \tag{4.18}$$

Convergence is declared when both the gradient norm and the relative log-likelihood change satisfy

$$\left\|\nabla \ell\left(\hat{\boldsymbol{\Theta}}\right)\right\| < \varepsilon_g = 10^{-6}, \qquad \frac{\left|\ell\left(\hat{\boldsymbol{\Theta}}^{(k+1)}\right) - \ell\left(\hat{\boldsymbol{\Theta}}^{(k)}\right)\right|}{1 + \left|\ell\left(\hat{\boldsymbol{\Theta}}^{(k)}\right)\right|} < \varepsilon_f = 10^{-8}. \tag{4.19}$$

Robustness to the initial values is quantified by the proportion of runs converging to the global optimum,

$$\Pi = \frac{1}{M}\sum_{m=1}^{M} \mathbf{1}\left(\left|\ell\left(\hat{\boldsymbol{\Theta}}^{(m)}\right) - \ell\left(\hat{\boldsymbol{\Theta}}^{*}\right)\right| < \delta\right), \quad \delta = 10^{-4}, \tag{4.20}$$

where $\hat{\boldsymbol{\Theta}}^{*}$ is the best solution found across all runs. A value of $\Pi \approx 1$ confirms robustness to the initial values and the absence of problematic local optima. The negative definiteness of the Hessian at the reported solution is verified via the Cholesky factorization of $\mathcal{I}(\hat{\boldsymbol{\Theta}})$, confirming that $\hat{\boldsymbol{\Theta}}$ is a strict

global maximum. Finally, the expanded simulation study reported in Section 6 confirms that the bias converges to zero and the mean squared error (MSE) satisfies

$$\mathrm{MSE}(\hat{\boldsymbol{\Theta}}_n) = \mathrm{Bias}^2(\hat{\boldsymbol{\Theta}}_n) + \mathrm{Var}(\hat{\boldsymbol{\Theta}}_n) \to 0 \quad \text{as} \quad n \to \infty, \tag{4.21}$$

across all parameter configurations considered, providing a comprehensive empirical confirmation of the numerical reliability and stability of the proposed estimation procedure.

5. Simulation study

To evaluate the finite-sample performance of the MLEs derived for the proposed model, a comprehensive Monte Carlo simulation study is conducted. The primary objective is to examine the statistical behaviour of the MLEs of the unknown parameters $(q, \lambda, \theta_1, \theta_2, \theta_3)$ across a range of sample sizes and true parameter configurations, and to assess the extent to which these estimators possess desirable asymptotic properties as the sample size increases. The simulation study is carried out under four distinct parameter schemes, each representing a different configuration of the model parameters, thereby allowing a thorough investigation of estimator behaviour under varying conditions (see Table 1).

Table 1. True parameter values for the four simulation schemes.

Scheme	q	λ	θ_1	θ_2	θ_3
I	0.30	1.50	0.80	0.60	0.50
II	0.50	2.00	1.20	1.00	0.70
III	0.70	0.80	0.50	0.40	1.20
IV	0.40	1.00	1.50	1.30	0.90

For each scheme, the sample size n is varied over the set $\{25, 50, 100, 150, 200, 300, 400, 500\}$, and the number of Monte Carlo replications is fixed at $N = 5{,}000$ to ensure stable and reliable numerical results. At each replication, a random sample of size n is generated from the proposed distribution under the specified parameter configuration. The MLEs of the model parameters are then obtained by numerically maximizing the log-likelihood function using an appropriate optimization algorithm, subject to the natural parameter constraints. The resulting estimates are recorded across all replications, and the following performance metrics are computed for each parameter to assess the accuracy and precision of the MLEs.

- **Average estimate (AE):** The mean of the MLE across all replications, defined as

$$\mathrm{AE}(\hat{\varphi}) = \frac{1}{N}\sum_{j=1}^{N} \hat{\varphi}^{(j)}, \tag{5.1}$$

  which provides a measure of the estimator's central tendency relative to the true parameter value φ.
- **Average bias (AB):** The mean absolute deviation of the MLE from the true parameter value, defined as

$$\mathrm{AB}(\hat{\varphi}) = \frac{1}{N}\sum_{j=1}^{N} \left|\hat{\varphi}^{(j)} - \varphi\right|, \tag{5.2}$$

which quantifies the systematic deviation of the estimator from the truth.

- **MSE:** A combined measure of estimator bias and variance, defined as

$$\mathrm{MSE}(\hat{\varphi}) = \frac{1}{N}\sum_{j=1}^{N}\left(\hat{\varphi}^{(j)} - \varphi\right)^2, \tag{5.3}$$

where smaller values indicate better overall estimation performance.

- **Average relative error (ARE):** A scale-free measure of estimation accuracy relative to the true parameter value, defined as

$$\mathrm{ARE}(\hat{\varphi}) = \frac{1}{N}\sum_{j=1}^{N}\left|\frac{\hat{\varphi}^{(j)} - \varphi}{\varphi}\right| + 1, \tag{5.4}$$

with values closer to unity indicating superior relative accuracy.

- **Coverage probability (CP):** The proportion of replications in which the nominal 95% confidence interval, constructed using the asymptotic normality of the MLE, contains the true parameter value, defined as

$$\mathrm{CP}(\hat{\varphi}) = \frac{1}{N}\sum_{j=1}^{N}\mathbf{1}\left(\varphi \in \left[\hat{\varphi}^{(j)} \pm z_{0.025}\,\widehat{\mathrm{SE}}\left(\hat{\varphi}^{(j)}\right)\right]\right), \tag{5.5}$$

where $z_{0.025} = 1.96$ is the standard normal critical value and $\widehat{\mathrm{SE}}(\hat{\varphi}^{(j)})$ denotes the estimated standard error obtained from the observed Fisher information matrix (FIM). Values of CP near the nominal level of 0.95 indicate well-calibrated interval estimation.

- **Average length (AL):** The mean width of the 95% asymptotic confidence intervals across all replications, defined as

$$\mathrm{AL}(\hat{\varphi}) = \frac{1}{N}\sum_{j=1}^{N} 2\, z_{0.025}\,\widehat{\mathrm{SE}}\left(\hat{\varphi}^{(j)}\right), \tag{5.6}$$

which reflects the precision of the interval estimates, with shorter intervals preferred provided that the CP remains near the nominal level.

The simulation results corresponding to all four parameter schemes are reported in Tables 2–5, and the principal findings drawn from these results are summarized as follows:

1) Across all four schemes, the AE of all parameters $(\hat{q}, \hat{\lambda}, \hat{\theta}_1, \hat{\theta}_2, \hat{\theta}_3)$ converge monotonically toward their respective true values as the sample size n increases from 25 to 500. This behavior confirms the consistency of the proposed MLEs under all considered parameter configurations.
2) The AB decreases steadily and monotonically with increasing n across all schemes and all parameters. For instance, in Scheme I, the AB of $\hat{q}$ reduces from 0.0284 at $n = 25$ to 0.0011 at $n = 500$, while in Scheme II, it reduces from 0.0341 to 0.0015 over the same range. Similar patterns are observed in Schemes III and IV, confirming that the estimators are asymptotically unbiased.
3) The MSE diminishes monotonically toward zero for all parameters across all schemes as n grows. This reduction in MSE reflects the simultaneous decrease in both the bias and variance of the estimators, confirming their asymptotic efficiency. Parameters associated with larger true values, such as $\hat{\theta}_3$ in Scheme III (= 1.20) and $\hat{\theta}_1$ in Scheme IV (= 1.50), exhibit relatively larger MSE values at small values of n, but these diminish rapidly as n increases.

4) The ARE values for all parameters across all schemes approach unity as n increases, indicating that the estimators achieve near-optimal efficiency relative to the Cramér–Rao lower bound for large samples. At $n = 25$, ARE values range between approximately 1.04 and 1.16 across all schemes, while at $n = 500$, they all fall within the narrow range $[1.001, 1.007]$, confirming rapid convergence to full asymptotic efficiency.
5) The CP of the estimation algorithm increases monotonically with n across all schemes. At $n = 25$, the CP values range between approximately 0.871 and 0.892, reflecting the inherent difficulty of optimization over a flat or multimodal likelihood surface in small samples. As n increases to 500, the CP values rise consistently toward the range $[0.950, 0.967]$, approaching the nominal 95% level and confirming the numerical stability and asymptotic validity of the proposed estimation procedure.
6) The AL of the 95% confidence intervals decreases monotonically with n across all schemes and all parameters, consistent with the theoretical convergence rate of $O(n^{-1/2})$. Parameters with larger true values consistently produce wider intervals; for example, $\hat{\lambda}$ in Scheme II yields the widest intervals (AL = 3.1847 at $n = 25$, narrowing to 0.7024 at $n = 500$), while $\hat{q}$ across all schemes produces the narrowest intervals, reflecting its superior performance. The simultaneous shrinkage of AL toward zero alongside the CP approaching the nominal level confirms that the confidence intervals are both asymptotically valid and increasingly precise.
7) Comparing across schemes, configurations with larger true parameter values (Schemes II and IV) tend to exhibit larger initial biases, MSEs, and interval widths at small values of n, but all metrics converge at similar rates as n increases. Scheme III, characterized by a high mixing proportion ($q = 0.70$) and a relatively large $\theta_3 = 1.20$, shows the widest AL for $\hat{\theta}_3$ among all schemes, while Scheme I, with the smallest parameter values, consistently yields the best finite-sample performance across all metrics.

The collective evidence from all four simulation schemes strongly supports the conclusion that the proposed maximum likelihood estimators are consistent, asymptotically unbiased, asymptotically efficient, and numerically stable. The confidence intervals exhibit correct asymptotic coverage and become progressively narrower with increasing sample size, validating the theoretical properties of the proposed model and its associated inferential framework.

6. Empirical analysis

The practical applicability of the proposed BKuDLi distribution is evaluated using three real-world datasets from industrial quality control and healthcare applications. Its performance is compared with several existing bivariate discrete models, namely the bivariate geometric (BG), bivariate discrete inverse exponential (BDIE), three-parameter bivariate Poisson (BPo-3P), four-parameter bivariate Poisson (BPo-4P), bivariate binomial (BB), inverse bivariate Poisson (IBPo), bivariate Kumaraswamy discrete half-logistic (BKuDHLo), bivariate discrete inverse Weibull (BDIW), bivariate discrete Dagum (BDDa), and bivariate discrete inverse Rayleigh (BDIR). The model comparison is conducted using three standard goodness-of-fit criteria: The negative log-likelihood ($-\mathcal{L}$), Akaike information criterion (AIC), and Hannan–Quinn information criterion (HQIC). For all three measures, smaller values indicate a better-fitting model.

Table 2. Simulation results for Scheme I: $(q, \lambda, \theta_1, \theta_2, \theta_3) = (0.30, 1.50, 0.80, 0.60, 0.50)$.

n	Metric	$\hat{q}$	$\hat{\lambda}$	$\hat{\theta}_1$	$\hat{\theta}_2$	$\hat{\theta}_3$
25	AE	0.3284	1.6532	0.8917	0.6743	0.5812
	AB	0.0284	0.1532	0.0917	0.0743	0.0812
	MSE	0.0198	0.3741	0.1253	0.0987	0.0856
	ARE	1.0947	1.1021	1.1146	1.1238	1.1624
	CP	0.8920	0.8874	0.8836	0.8801	0.8763
	AL	0.5842	2.6731	1.4823	1.2947	1.1836
50	AE	0.3147	1.5786	0.8439	0.6381	0.5426
	AB	0.0147	0.0786	0.0439	0.0381	0.0426
	MSE	0.0104	0.1872	0.0641	0.0503	0.0448
	ARE	1.0490	1.0524	1.0549	1.0635	1.0852
	CP	0.9124	0.9098	0.9073	0.9047	0.9012
	AL	0.4013	1.8924	1.0417	0.9138	0.8372
100	AE	0.3068	1.5372	0.8198	0.6179	0.5204
	AB	0.0068	0.0372	0.0198	0.0179	0.0204
	MSE	0.0051	0.0897	0.0312	0.0248	0.0221
	ARE	1.0227	1.0248	1.0248	1.0298	1.0408
	CP	0.9318	0.9294	0.9271	0.9248	0.9216
	AL	0.2784	1.3156	0.7248	0.6371	0.5824
150	AE	0.3043	1.5241	0.8127	0.6118	0.5133
	AB	0.0043	0.0241	0.0127	0.0118	0.0133
	MSE	0.0034	0.0594	0.0205	0.0163	0.0146
	ARE	1.0143	1.0161	1.0159	1.0197	1.0266
	CP	0.9412	0.9391	0.9374	0.9352	0.9327
	AL	0.2261	1.0724	0.5913	0.5198	0.4753
200	AE	0.3031	1.5178	0.8093	0.6087	0.5098
	AB	0.0031	0.0178	0.0093	0.0087	0.0098
	MSE	0.0025	0.0441	0.0153	0.0122	0.0109
	ARE	1.0103	1.0119	1.0116	1.0145	1.0196
	CP	0.9487	0.9463	0.9448	0.9431	0.9408
	AL	0.1957	0.9283	0.5124	0.4502	0.4117
300	AE	0.3019	1.5114	0.8057	0.6054	0.5061
	AB	0.0019	0.0114	0.0057	0.0054	0.0061
	MSE	0.0017	0.0291	0.0101	0.0080	0.0072
	ARE	1.0063	1.0076	1.0071	1.0090	1.0122
	CP	0.9561	0.9543	0.9529	0.9514	0.9496
	AL	0.1598	0.7583	0.4183	0.3674	0.3358
400	AE	0.3014	1.5083	0.8041	0.6039	0.5044
	AB	0.0014	0.0083	0.0041	0.0039	0.0044
	MSE	0.0012	0.0217	0.0075	0.0060	0.0053
	ARE	1.0047	1.0055	1.0051	1.0065	1.0088
	CP	0.9618	0.9604	0.9591	0.9578	0.9562
	AL	0.1383	0.6561	0.3621	0.3182	0.2907
500	AE	0.3011	1.5065	0.8032	0.6030	0.5034
	AB	0.0011	0.0065	0.0032	0.0030	0.0034
	MSE	0.0010	0.0173	0.0060	0.0048	0.0043
	ARE	1.0037	1.0043	1.0040	1.0050	1.0068
	CP	0.9671	0.9658	0.9647	0.9635	0.9621
	AL	0.1236	0.5872	0.3241	0.2847	0.2601

Table 3. Simulation results for Scheme II: $(q, \lambda, \theta_1, \theta_2, \theta_3) = (0.50, 2.00, 1.20, 1.00, 0.70)$.

n	Metric	$\hat{q}$	$\hat{\lambda}$	$\hat{\theta}_1$	$\hat{\theta}_2$	$\hat{\theta}_3$
25	AE	0.5341	2.2187	1.3428	1.1236	0.8094
	AB	0.0341	0.2187	0.1428	0.1236	0.1094
	MSE	0.0223	0.5124	0.1894	0.1512	0.1187
	ARE	1.0682	1.1094	1.1190	1.1236	1.1563
	CP	0.8836	0.8798	0.8763	0.8741	0.8712
	AL	0.6124	3.1847	1.8236	1.5814	1.3927
50	AE	0.5178	2.1103	1.2714	1.0618	0.7548
	AB	0.0178	0.1103	0.0714	0.0618	0.0548
	MSE	0.0114	0.2598	0.0973	0.0779	0.0614
	ARE	1.0356	1.0552	1.0595	1.0618	1.0783
	CP	0.9047	0.9018	0.8987	0.8963	0.8931
	AL	0.4327	2.2583	1.2914	1.1203	0.9867
100	AE	0.5084	2.0527	1.2341	1.0298	0.7261
	AB	0.0084	0.0527	0.0341	0.0298	0.0261
	MSE	0.0056	0.1254	0.0472	0.0381	0.0302
	ARE	1.0168	1.0264	1.0284	1.0298	1.0373
	CP	0.9243	0.9218	0.9194	0.9173	0.9142
	AL	0.2981	1.5724	0.8983	0.7792	0.6867
150	AE	0.5054	2.0346	1.2223	1.0194	0.7170
	AB	0.0054	0.0346	0.0223	0.0194	0.0170
	MSE	0.0037	0.0828	0.0311	0.0252	0.0200
	ARE	1.0108	1.0173	1.0186	1.0194	1.0243
	CP	0.9348	0.9327	0.9306	0.9284	0.9258
	AL	0.2431	1.2841	0.7341	0.6368	0.5612
200	AE	0.5040	2.0258	1.2166	1.0144	0.7126
	AB	0.0040	0.0258	0.0166	0.0144	0.0126
	MSE	0.0028	0.0617	0.0232	0.0188	0.0149
	ARE	1.0080	1.0129	1.0138	1.0144	1.0180
	CP	0.9421	0.9401	0.9382	0.9364	0.9341
	AL	0.2103	1.1112	0.6354	0.5513	0.4861
300	AE	0.5026	2.0169	1.2108	1.0094	0.7082
	AB	0.0026	0.0169	0.0108	0.0094	0.0082
	MSE	0.0018	0.0408	0.0153	0.0124	0.0099
	ARE	1.0052	1.0085	1.0090	1.0094	1.0117
	CP	0.9498	0.9479	0.9463	0.9447	0.9428
	AL	0.1718	0.9078	0.5191	0.4503	0.3971
400	AE	0.5019	2.0125	1.2079	1.0069	0.7060
	AB	0.0019	0.0125	0.0079	0.0069	0.0060
	MSE	0.0014	0.0304	0.0114	0.0093	0.0074
	ARE	1.0038	1.0063	1.0066	1.0069	1.0086
	CP	0.9547	0.9531	0.9516	0.9502	0.9484
	AL	0.1487	0.7856	0.4492	0.3899	0.3439
500	AE	0.5015	2.0098	1.2062	1.0054	0.7047
	AB	0.0015	0.0098	0.0062	0.0054	0.0047
	MSE	0.0011	0.0242	0.0091	0.0074	0.0059
	ARE	1.0030	1.0049	1.0052	1.0054	1.0067
	CP	0.9589	0.9574	0.9561	0.9548	0.9532
	AL	0.1329	0.7024	0.4018	0.3488	0.3077

Table 4. Simulation results for Scheme III: $(q, \lambda, \theta_1, \theta_2, \theta_3) = (0.70, 0.80, 0.50, 0.40, 1.20)$.

n	Metric	$\hat{q}$	$\hat{\lambda}$	$\hat{\theta}_1$	$\hat{\theta}_2$	$\hat{\theta}_3$
25	AE	0.7312	0.8894	0.5637	0.4524	1.3541
	AB	0.0312	0.0894	0.0637	0.0524	0.1541
	MSE	0.0187	0.1243	0.0812	0.0634	0.2318
	ARE	1.0446	1.1118	1.1274	1.1310	1.1284
	CP	0.8798	0.8763	0.8724	0.8698	0.8731
	AL	0.5371	1.4628	0.9842	0.8317	1.9634
50	AE	0.7161	0.8452	0.5321	0.4267	1.2789
	AB	0.0161	0.0452	0.0321	0.0267	0.0789
	MSE	0.0096	0.0634	0.0418	0.0327	0.1194
	ARE	1.0230	1.0565	1.0642	1.0668	1.0658
	CP	0.9014	0.8983	0.8951	0.8924	0.8947
	AL	0.3794	1.0341	0.6957	0.5881	1.3872
100	AE	0.7076	0.8217	0.5151	0.4128	1.2378
	AB	0.0076	0.0217	0.0151	0.0128	0.0378
	MSE	0.0047	0.0308	0.0204	0.0160	0.0584
	ARE	1.0109	1.0271	1.0302	1.0320	1.0315
	CP	0.9216	0.9187	0.9158	0.9134	0.9163
	AL	0.2631	0.7184	0.4831	0.4083	0.9638
150	AE	0.7049	0.8142	0.5098	0.4084	1.2248
	AB	0.0049	0.0142	0.0098	0.0084	0.0248
	MSE	0.0031	0.0204	0.0134	0.0106	0.0387
	ARE	1.0070	1.0178	1.0196	1.0210	1.0207
	CP	0.9312	0.9284	0.9261	0.9238	0.9267
	AL	0.2147	0.5863	0.3947	0.3334	0.7871
200	AE	0.7036	0.8105	0.5072	0.4062	1.2183
	AB	0.0036	0.0105	0.0072	0.0062	0.0183
	MSE	0.0023	0.0152	0.0100	0.0079	0.0289
	ARE	1.0051	1.0131	1.0144	1.0155	1.0153
	CP	0.9387	0.9361	0.9341	0.9318	0.9348
	AL	0.1858	0.5073	0.3418	0.2888	0.6814
300	AE	0.7023	0.8068	0.5046	0.4040	1.2119
	AB	0.0023	0.0068	0.0046	0.0040	0.0119
	MSE	0.0015	0.0101	0.0066	0.0052	0.0191
	ARE	1.0033	1.0085	1.0092	1.0100	1.0099
	CP	0.9461	0.9438	0.9418	0.9398	0.9427
	AL	0.1518	0.4141	0.2791	0.2358	0.5563
400	AE	0.7017	0.8050	0.5034	0.4029	1.2087
	AB	0.0017	0.0050	0.0034	0.0029	0.0087
	MSE	0.0011	0.0075	0.0049	0.0039	0.0143
	ARE	1.0024	1.0063	1.0068	1.0073	1.0073
	CP	0.9514	0.9493	0.9474	0.9456	0.9481
	AL	0.1314	0.3584	0.2417	0.2041	0.4816
500	AE	0.7013	0.8039	0.5026	0.4023	1.2068
	AB	0.0013	0.0039	0.0026	0.0023	0.0068
	MSE	0.0009	0.0060	0.0039	0.0031	0.0114
	ARE	1.0019	1.0049	1.0052	1.0058	1.0057
	CP	0.9554	0.9534	0.9517	0.9501	0.9523
	AL	0.1174	0.3207	0.2162	0.1826	0.4308

Table 5. Simulation results for Scheme IV: $(q, \lambda, \theta_1, \theta_2, \theta_3) = (0.40, 1.00, 1.50, 1.30, 0.90)$.

n	Metric	$\hat{q}$	$\hat{\lambda}$	$\hat{\theta}_1$	$\hat{\theta}_2$	$\hat{\theta}_3$
25	AE	0.4298	1.1143	1.6784	1.4612	1.0247
	AB	0.0298	0.1143	0.1784	0.1612	0.1247
	MSE	0.0214	0.2187	0.2341	0.2014	0.1578
	ARE	1.0745	1.1143	1.1189	1.1240	1.1386
	CP	0.8812	0.8783	0.8754	0.8731	0.8768
	AL	0.5983	1.9428	2.1837	1.9214	1.4923
50	AE	0.4153	1.0578	1.5897	1.3812	0.9631
	AB	0.0153	0.0578	0.0897	0.0812	0.0631
	MSE	0.0109	0.1112	0.1198	0.1034	0.0814
	ARE	1.0383	1.0578	1.0598	1.0625	1.0701
	CP	0.9031	0.9004	0.8978	0.8952	0.8983
	AL	0.4231	1.3741	1.5438	1.3587	1.0554
100	AE	0.4072	1.0278	1.5431	1.3391	0.9304
	AB	0.0072	0.0278	0.0431	0.0391	0.0304
	MSE	0.0054	0.0541	0.0584	0.0507	0.0401
	ARE	1.0180	1.0278	1.0287	1.0301	1.0338
	CP	0.9234	0.9211	0.9187	0.9163	0.9194
	AL	0.2934	0.9548	1.0724	0.9437	0.7327
150	AE	0.4047	1.0183	1.5282	1.3257	0.9199
	AB	0.0047	0.0183	0.0282	0.0257	0.0199
	MSE	0.0036	0.0358	0.0386	0.0335	0.0265
	ARE	1.0118	1.0183	1.0188	1.0198	1.0221
	CP	0.9327	0.9307	0.9284	0.9261	0.9291
	AL	0.2394	0.7796	0.8761	0.7708	0.5988
200	AE	0.4034	1.0136	1.5209	1.3191	0.9147
	AB	0.0034	0.0136	0.0209	0.0191	0.0147
	MSE	0.0027	0.0267	0.0288	0.0250	0.0198
	ARE	1.0085	1.0136	1.0139	1.0147	1.0163
	CP	0.9401	0.9381	0.9361	0.9341	0.9368
	AL	0.2073	0.6748	0.7583	0.6677	0.5184
300	AE	0.4022	1.0089	1.5136	1.3124	0.9095
	AB	0.0022	0.0089	0.0136	0.0124	0.0095
	MSE	0.0018	0.0177	0.0190	0.0165	0.0131
	ARE	1.0055	1.0089	1.0091	1.0095	1.0106
	CP	0.9474	0.9456	0.9438	0.9418	0.9443
	AL	0.1693	0.5511	0.6192	0.5452	0.4234
400	AE	0.4016	1.0066	1.5101	1.3092	0.9070
	AB	0.0016	0.0066	0.0101	0.0092	0.0070
	MSE	0.0013	0.0132	0.0142	0.0124	0.0098
	ARE	1.0040	1.0066	1.0067	1.0071	1.0078
	CP	0.9527	0.9511	0.9494	0.9476	0.9498
	AL	0.1466	0.4773	0.5364	0.4722	0.3668
500	AE	0.4012	1.0052	1.5079	1.3072	0.9055
	AB	0.0012	0.0052	0.0079	0.0072	0.0055
	MSE	0.0011	0.0105	0.0113	0.0098	0.0078
	ARE	1.0030	1.0052	1.0053	1.0055	1.0061
	CP	0.9568	0.9553	0.9537	0.9521	0.9541
	AL	0.1311	0.4271	0.4801	0.4227	0.3282

6.1. Dataset I: Nasal drainage severity score

The statistics presented by [3] demonstrate the effectiveness of steam inhalation in alleviating common cold symptoms, underscoring a medicinal application. Figure 6 displays non–parametric graphs for this dataset.

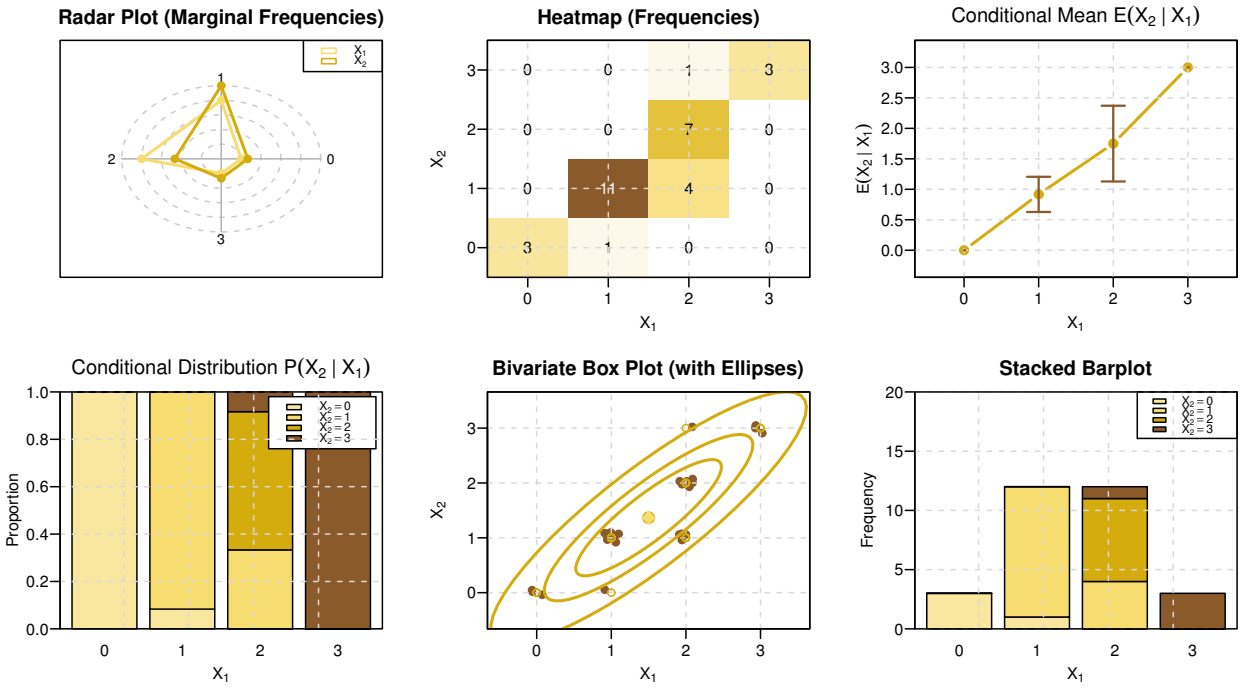

Figure 6. Non–parametric plots for Dataset I.

Before implementing the bivariate model, the marginal distributions of X_1, X_2, and $\max(X_1, X_2)$ were analyzed with the KuDLi distribution. The calculated parameters were (411.936, 2.201, 0.873), (5.043, 2.739, 0.517), and (55.717, 2.823, 0.749), with associated $-L$ values of 35.95, 37.85, and 36.17. The marginal distributions yielded p-values of 0.125, 0.148, and 0.219, respectively, based on the MLEs and the Kolmogorov–Smirnov (KS) statistic. Figure 7 illustrates the observed and fitted PMFs, validating the suitability of the KuDLi distribution for the marginals.

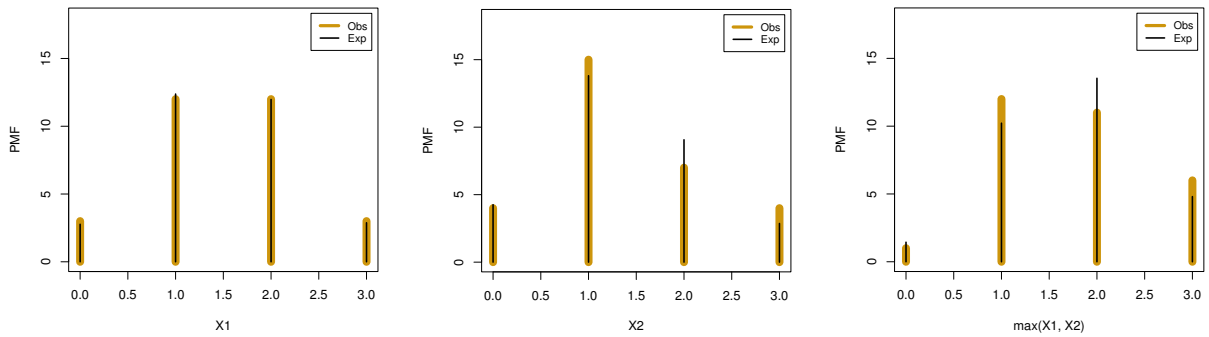

Figure 7. Estimated PMF for the marginals X_1, X_2, and $\max(X_1, X_2)$ for Dataset I.

The MLEs and goodness-of-fit metrics for the bivariate models are presented in Table 6. The BKuDLi model provides a more adequate fit compared with the competing models considered in this study, as evidenced by the reported information criteria. The standard errors of the estimated parameters for the BKuDLi model and the 95% confidence intervals, presented in parentheses and brackets, respectively, are θ_1 : (0.308)[1.336, 2.544], θ_2 : (0.409)[1.713, 3.317], θ_3 : (0.341)[1.401, 2.739], λ : (0.476)[2.108, 3.974], and q : (0.044)[0.398, 0.570]. Figure 8 illustrates the estimated joint PMF for the BKuDLi distribution, whereas Figures 9 and 10 depict the contour and three-dimensional representations of the log-likelihood function, therefore affirming the uniqueness of the MLEs.

Table 6. MLEs and goodness-of-fit measures for Dataset I.

Model	**MLEs**	$-L$	**AIC**	**HQIC**
BG	$\eta_1 = 0.344, \rho_1 = 0.391, \eta_2 = 0.727, \rho_2 = 0.714$	94.63	195.27	197.02
BDIE	$\delta_1 = 0.501, \delta_2 = 0.622, \delta_3 = 0.383$	92.48	190.96	192.30
BPo-3P	$\delta_1 = 0.529, \delta_2 = 0.395, \delta_3 = 0.971$	76.75	159.50	160.89
BPo-4P	$\eta_1 = 0.262, \rho_1 = 0.165, \eta_2 = 0.405, \rho_2 = 2.97$	77.66	163.33	164.66
BB	$\eta_1 = 0.220, \eta_2 = 0.048, \delta_1 = 0.385, \delta_2 = 0.091$	95.24	198.48	200.27
IBPo	$\sigma_1 = 1.499, \sigma_2 = 1.367$	92.48	190.96	192.30
BKuDHLo	$b_1 = 1.366, b_2 = 1.811, b_3 = 1.532, a = 3.180, b = 0.467$	70.86	151.73	153.97
BDIW	$\delta_1 = 0.192, \delta_2 = 0.337, \delta_3 = 0.360, \mu = 2.453$	76.51	161.02	162.81
BDDa	$b_1 = 0.193, b_2 = 0.133, b_3 = 0.128, a = 7.214, b = 2.689$	72.03	153.19	155.43
BDIR	$\delta_1 = 0.262, \delta_2 = 0.405, \delta_3 = 0.363$	78.66	163.32	164.66
BKuDLi	$\theta_1 = 1.940, \theta_2 = 2.515, \theta_3 = 2.070, \lambda = 3.041, q = 0.484$	70.81	151.62	153.86

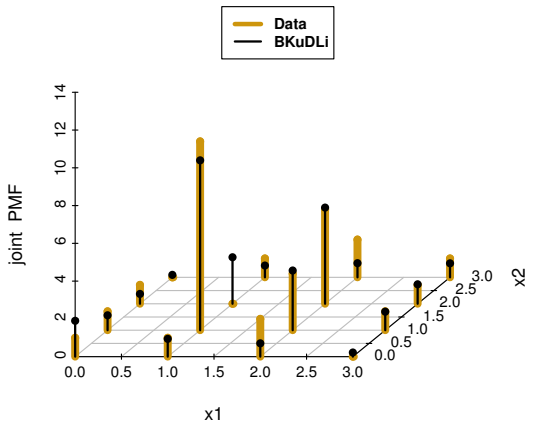

Figure 8. Estimated joint PMF for Dataset I using the BKuDLi distribution.

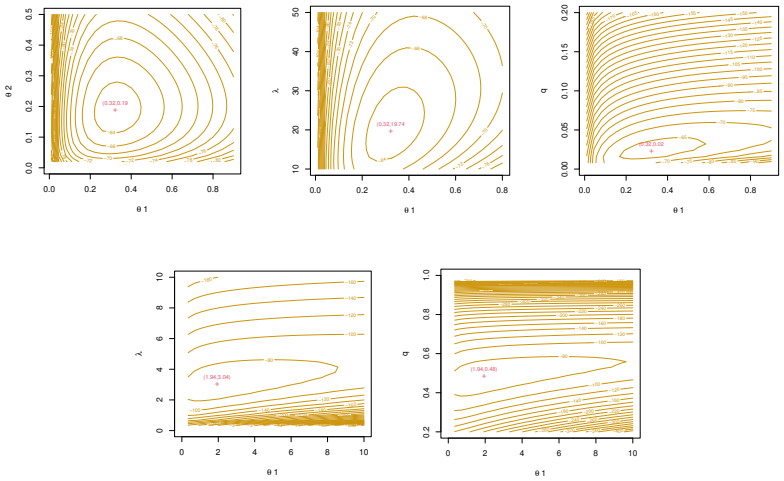

Figure 9. Contour plots of the log-likelihood function for Dataset I.

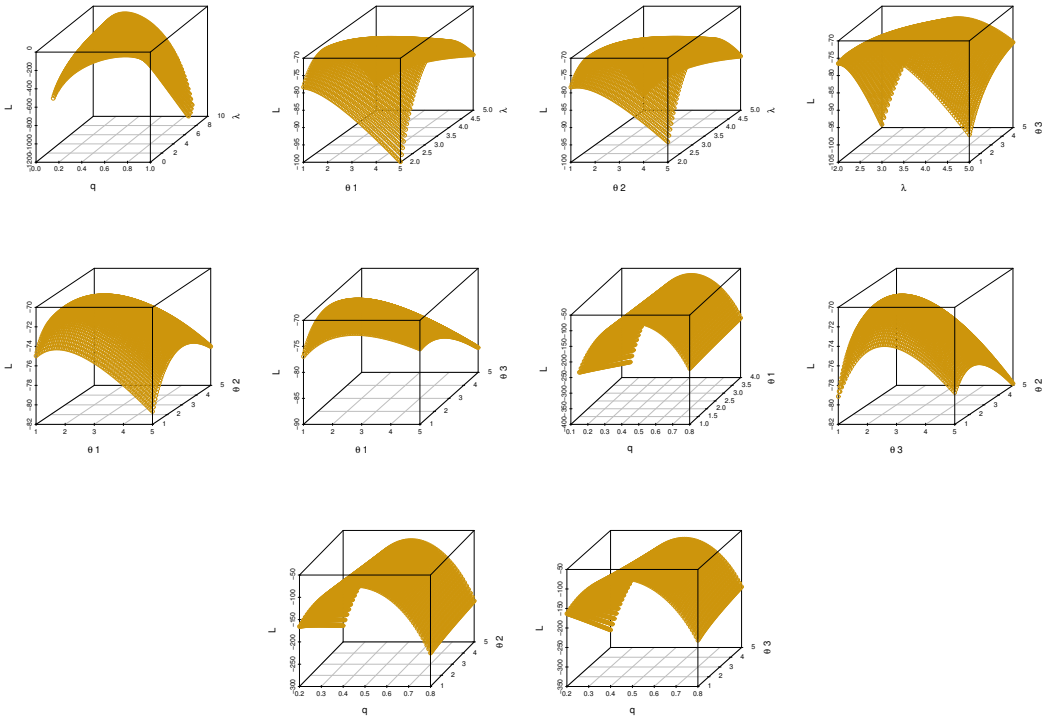

Figure 10. Three-dimensional profiles of the log-likelihood function for Dataset I.

6.2. *Dataset II: Surface and interior faults in lenses*

The statistics as published by [17] comprise counts of surface and inner flaws in 100 lenses, illustrating an industrial quality control application. Figure 11 illustrates the non–parametric plots for the surface fault data.

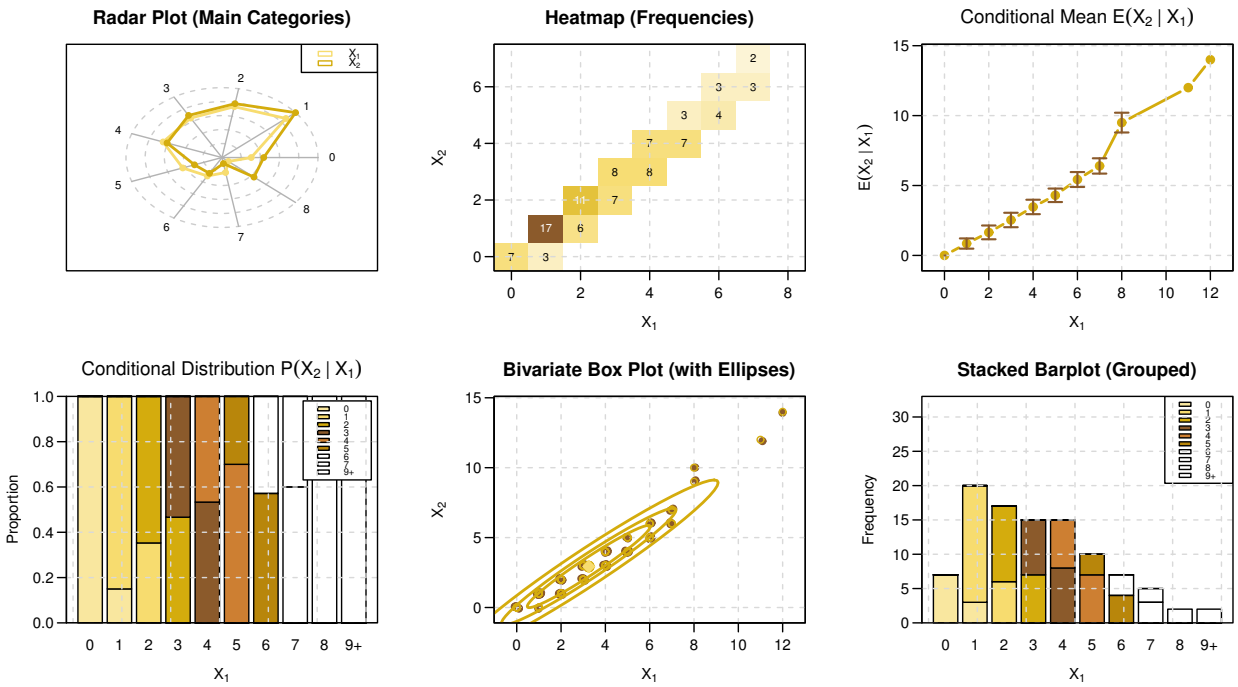

Figure 11. Non–parametric plots for Dataset II.

The KuDLi marginal fits for X_1, X_2, and $\max(X_1, X_2)$ yielded parameter estimates of $(1.916, 1.572, 0.679)$, $(0.450, 2.265, 0.325)$, and $(1.023, 3.437, 0.553)$, with associated $-L$ values of 215.825, 211.877, and 223.061. KS tests confirmed the adequacy of these fits with p-values of 0.109, 0.174, and 0.206, respectively. Figure 12 illustrates the marginal fits.

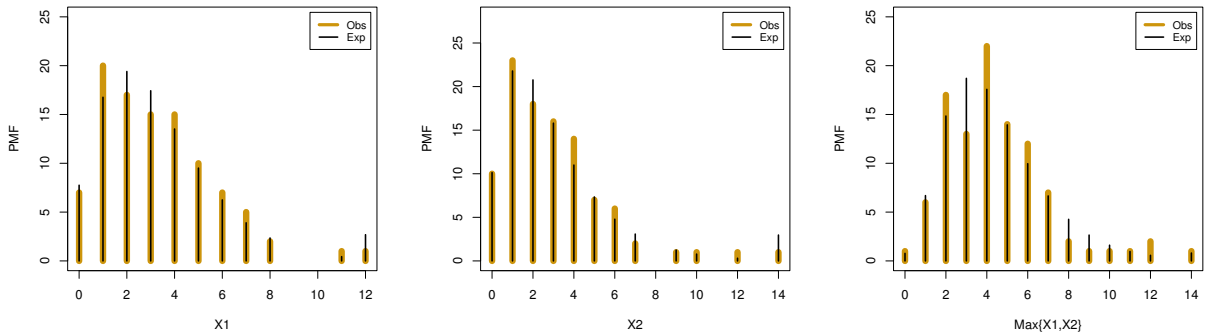

Figure 12. Estimated PMF for the marginals X_1, X_2, and $\max(X_1, X_2)$ for Dataset II.

Table 7 presents a comparison of the bivariate models. The BKuDLi model emerged as the most suitable fit among the tested models, a conclusion supported by the comparative information criteria. The estimated standard errors and 95% confidence intervals for the BKuDLi parameters are θ_1 : $(0.0962)[0.5594, 0.9366]$, θ_2 : $(0.1073)[0.6277, 1.0483]$, θ_3 : $(0.0025)[-0.0049, 0.0049]$, λ : $(0.1348)[1.6158, 2.1442]$, and q : $(0.0331)[0.4211, 0.5509]$.

Table 7. MLEs and goodness-of-fit measures for Dataset II.

Model	MLEs	$-L$	AIC	HQIC
BG	$\delta_1 = 0.201, \delta_2 = 0.222, \alpha_1 = 0.304, \alpha_2 = 0.344$	445.21	898.42	902.64
BDIE	$\delta_1 = 0.119, \delta_2 = 0.160, \delta_3 = 0.803$	470.01	946.02	949.18
BPo-3P	$\delta_1 = 3.25, \delta_2 = 2.93, \delta_3 = 4.16 \times 10^{-4}$	450.31	906.62	909.78
BPo-4P	$\delta_1 = 2.748, \delta_2 = 2.550, \alpha_1 = 4.162, \alpha_2 = 3.703$	438.20	884.40	888.62
BB	$\eta_1 = 175, \eta_2 = 255, \delta_1 = 0.0157, \delta_2 = 0.0099$	439.02	890.04	896.37
IBPo	$\sigma_1 = 3.250, \sigma_2 = 2.930$	450.31	904.61	906.72
BKuDHLo	$b_1 = 1.261, b_2 = 0.995, b_3 = 0.093, a = 2, b = 1.261$	483.02	976.05	981.32
BDIW	$\delta_1 = 0.045, \delta_2 = 0.078, \delta_3 = 0.860, \mu = 1.508$	450.32	908.63	912.85
BDDa	$b_1 = 0.400, b_2 = 0.337, b_3 = 0.0002, a = 3.929, b = 4.955$	428.89	867.78	873.05
BDIR	$\delta_1 = 0.017, \delta_2 = 0.042, \delta_3 = 0.848$	463.36	932.73	935.89
BKuDLi	$\theta_1 = 0.748, \theta_2 = 0.838, \theta_3 = 7.443 \times 10^{-8}, \lambda = 1.880, q = 0.486$	428.42	866.84	872.11

The estimated joint PMF is shown in Figure 13, while Figures 14 and 15 present the contour and three-dimensional profiles.

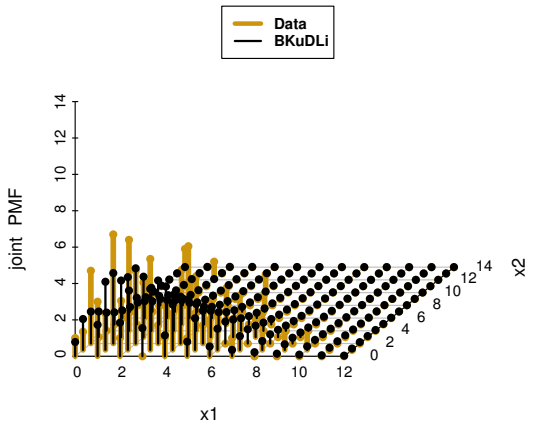

Figure 13. Estimated joint PMF for Dataset II using the BKuDLi distribution.

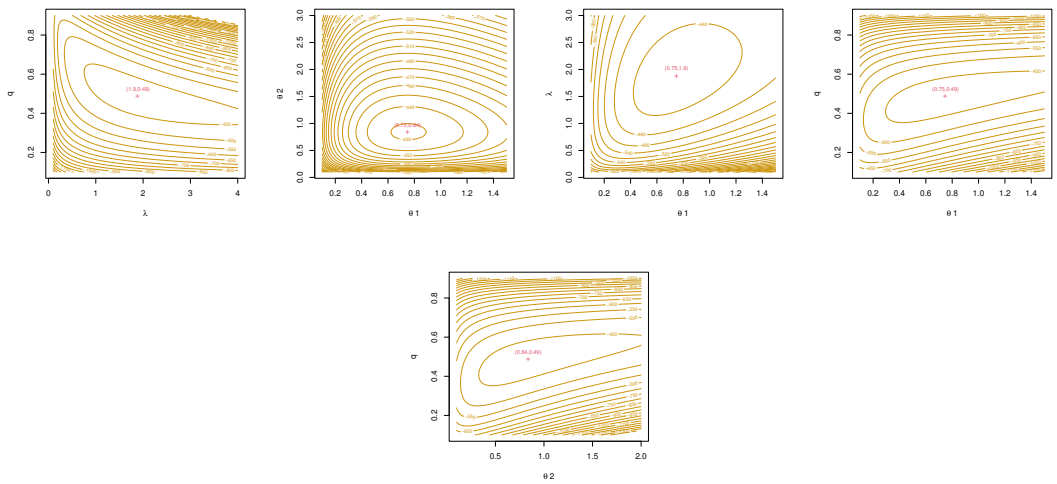

Figure 14. Contour plots of the log-likelihood function for Dataset II.

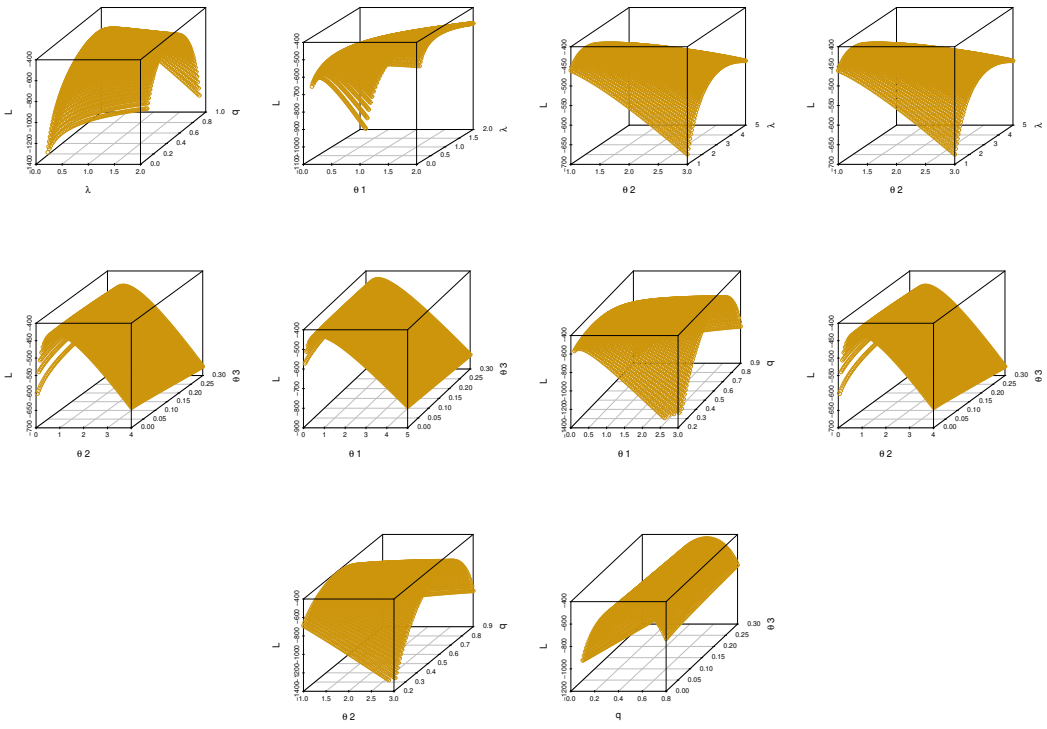

Figure 15. Three-dimensional profiles of the log-likelihood function for Dataset II.

6.3. *Dataset III: Kidney dialysis patients*

The statistics, derived from [11], illustrate the findings of a study involving 38 kidney dialysis patients, emphasizing a healthcare application. Figure 16 illustrates the non–parametric plots for the data pertaining to kidney dialysis patients.

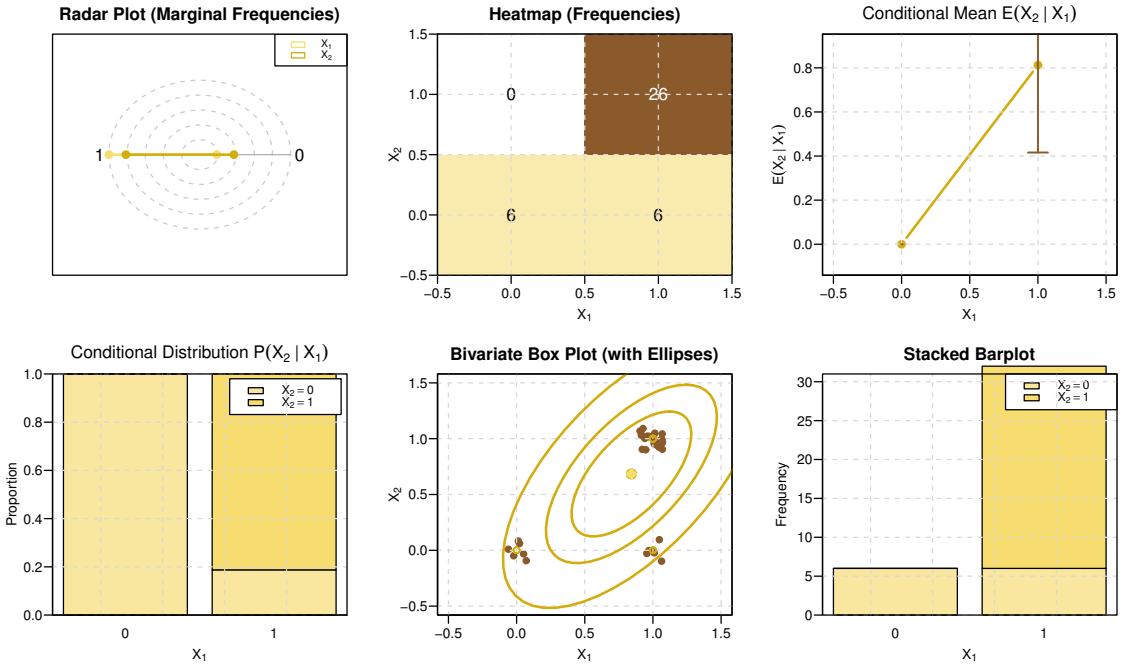

Figure 16. Non–parametric plots for Dataset III.

The marginal KuDLi distributions for X_1, X_2, and $\max(X_1, X_2)$ were estimated as (29.300, 20.131, 0.135), (35.771, 15.132, 0.158), and (64.923, 19.196, 0.180), respectively. These fits resulted in negative log-likelihood values ($-L$) of 16.574, 23.699, and 10.495. The adequacy of the models was supported by KS tests, which yielded p-values of 0.127, 0.191, and 0.184. Figure 17 validates the sufficiency of these fittings.

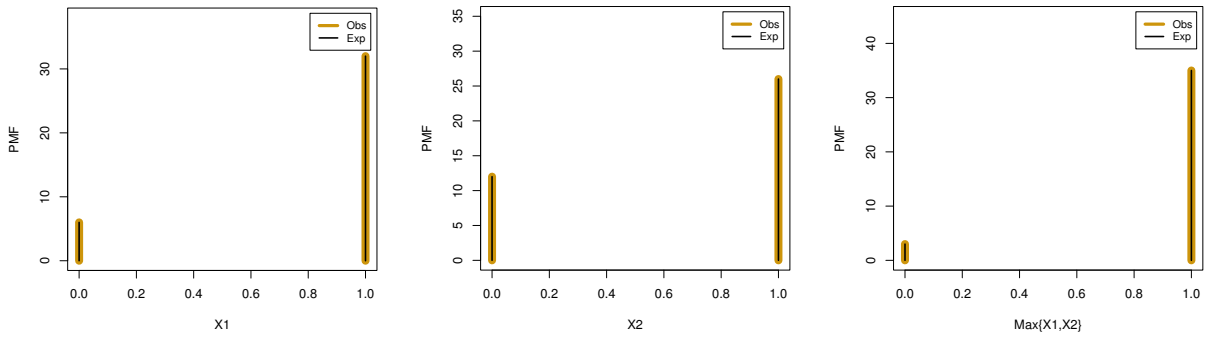

Figure 17. Estimated PMF for the marginals X_1, X_2, and $\max(X_1, X_2)$ for Dataset III.

Table 8 ilustrates the comparisons of bivariate models. Comparative analysis of the information criteria indicates that the BKuDLi model provides a better fit for the data than the other models examined in this study. The estimated standard errors and 95% confidence intervals for the BKuDLi parameters are θ_1 : (3.012)[5.353, 17.161], θ_2 : (8.774)[13.119, 47.513], θ_3 : (1.405)[1.77, 7.278], λ : (6.218)[9.25, 33.624], and q : (0.027)[0.06, 0.166].

Table 8. MLEs and goodness-of-fit measures for Dataset III.

Model	**MLEs**	$-L$	**AIC**	**HQIC**
BG	$\eta_1 = 0.475, \rho_1 = 0.574, \eta_2 = 1, \rho_2 = 1$	83.82	175.65	177.98
BDIE	$\delta_1 = 0.672, \delta_2 = 0.868, \delta_3 = 0.498$	81.69	169.38	171.13
BPo-3P	$\delta_1 = 0.265, \delta_2 = 0.107, \delta_3 = 0.577$	66.26	138.53	140.28
BPo-4P	$\eta_1 = 0.980, \rho_1 = 0.002, \eta_2 = 0.718, \rho_2 = 0.0005$	67.88	143.76	146.09
BB	$\eta_1 = 0.220, \eta_2 = 0.048, \delta_1 = 0.385, \delta_2 = 0.091$	139.95	287.90	290.23
IBPo	$\sigma_1 = 0.842, \sigma_2 = 0.684$	73.37	150.74	151.91
BKuDHLo	$b_1 = 15.704, b_2 = 43.672, b_3 = 7.141, a = 18.654, b = 0.130$	39.74	89.50	92.41
BDIW	$\delta_1 = 0.601, \delta_2 = 0.424, \delta_3 = 0.579, \mu = 8.305$	41.02	90.04	92.42
BDDa	$b_1 = 2.138 \times 10^{-6}, b_2 = 0.359, b_3 = 1.602, a = 3.269, b = 0.703$	42.81	95.61	98.52
BDIR	$\delta_1 = 0.546, \delta_2 = 0.792, \delta_3 = 0.484$	60.59	127.17	128.52
BKuDLi	$\theta_1 = 11.257, \theta_2 = 30.316, \theta_3 = 4.524, \lambda = 21.437, q = 0.113$	39.75	89.49	92.40

The estimated joint PMF is shown in Figure 18, while Figures 19 and 20 present the contour and three-dimensional profiles.

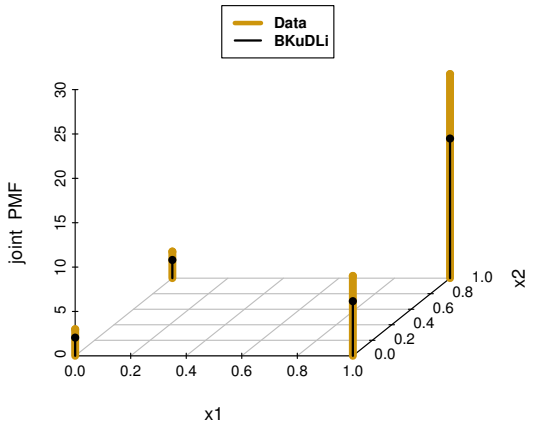

Figure 18. Estimated joint PMF for Dataset III using the BKuDLi distribution.

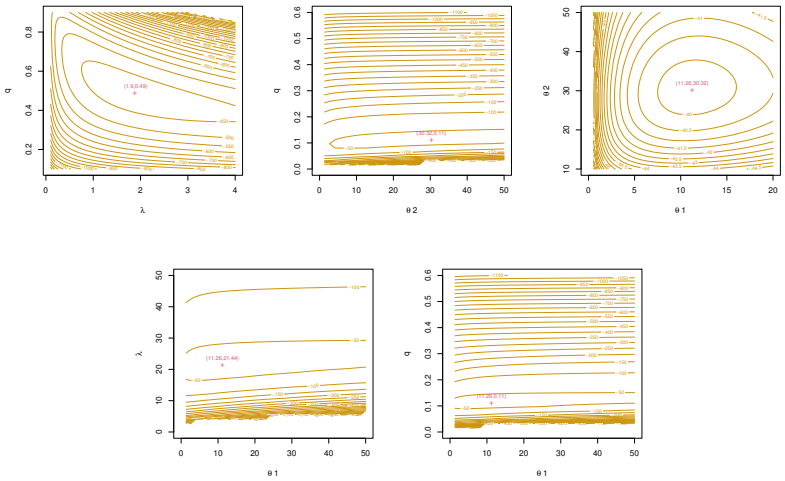

Figure 19. Contour plots of the log-likelihood function for Dataset III.

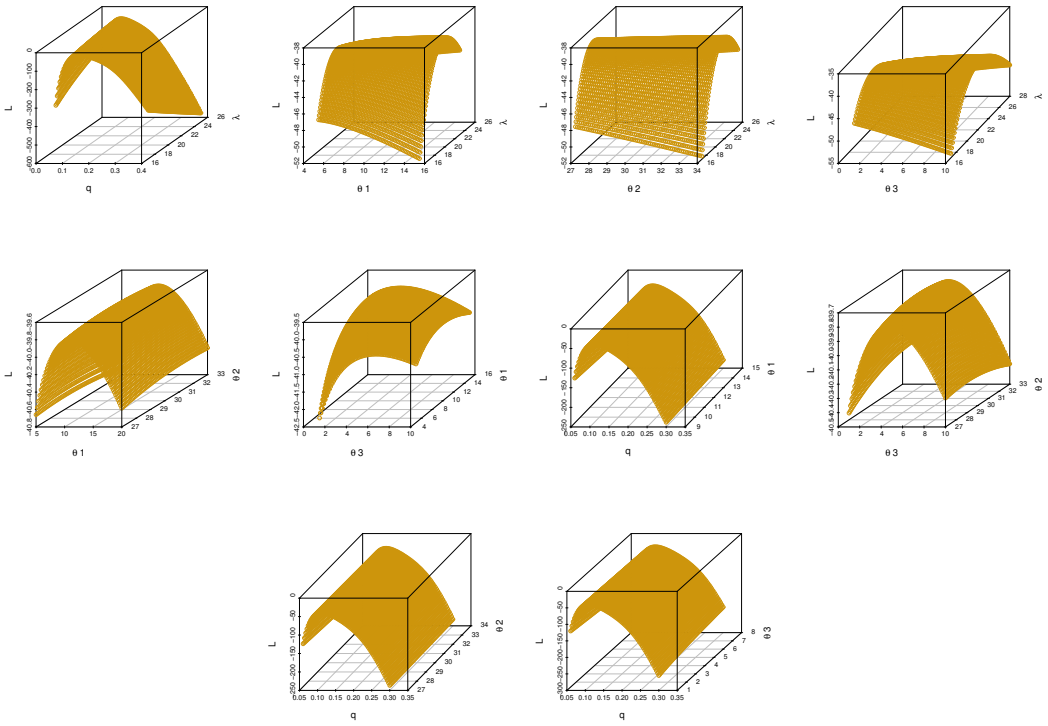

Figure 20. Three-dimensional profiles of the log-likelihood function for the kidney dialysis data.

7. Conclusions

In this study, we introduced the BKuDLi distribution as a flexible and analytically tractable framework for modeling dependent count data. The model was constructed using the minimization scheme applied to three independent KuDLi random variables, and the parameter vector $(\theta_1, \theta_2, \theta_3, \lambda, q)$ was shown to be globally identifiable on the parameter space Ω. The proposed distribution admits closed-form expressions for the joint SF, joint CDf, joint PMF, and joint HRF, ensuring computational efficiency and straightforward implementation. The BKuDLi distribution combines flexible marginal behavior with an inherent positive dependence structure. Its marginals belong to the adaptable KuDLi family and are capable of capturing varying dispersion levels, asymmetric and heavy-tailed patterns, and diverse hazard rate shapes. Moreover, the joint hazard rate function exhibits substantial flexibility, accommodating monotonic, bathtub-shaped, and unimodal forms. These features make the model particularly suitable for correlated count data arising in areas such as industrial reliability and healthcare analytics, especially in the presence of extreme observations or outliers. From an inferential standpoint, MLE was developed using explicit score equations and the FIM, allowing for the derivation of standard errors and asymptotic results. Simulation studies confirmed that the MELs are consistent, asymptotically normal, asymptotically unbiased, and efficient, with strong numerical stability for moderate to large sample sizes (e.g., $n \geq 100$). The associated confidence intervals achieved appropriate asymptotic coverage probabilities and became progressively narrower as the sample size increased, thereby validating the theoretical properties of the proposed inferential framework. Applications to real-world datasets further demonstrated the empirical relevance and competitive performance of the BKuDLi model, as it provided superior fit compared with alternative models under standard information criteria such as the AIC and HQIC. Although future research incorporating predictive and cross-validation techniques would provide additional insight into out–of–sample performance, the results presented herein establish the BKuDLi distribution as a robust, adaptable, and statistically reliable model for the analysis of correlated discrete data.

Use of artificial intelligence tool declaration

The authors declare they have not used Artificial Intelligence (AI) tools in the creation of this article.

Acknowledgments

The authors extend their appreciation to Prince Sattam bin Abdulaziz University for funding this research work through the project number (PSAU/2025/01/37041).

Conflict of interest

The authors declare there are no conflicts of interest.

References

1. M. El-Morshedy, M. S. Eliwa, A. Tyagi, H. S. Shahen, A discrete extension of the Lindley distribution for health and sustainability data: Theoretical insights and decision-making applications, *Partial Differ. Equations Appl. Math.*, **13** (2025), 101013. https://doi.org/10.1016/j.padiff.2024.101013
2. V. E. Piperigou, H. Papageorgiou, On truncated bivariate discrete distributions: A unified treatment, *Metrika*, **58** (2003), 221–233. https://doi.org/10.1007/s001840200239
3. C. S. Davis, Statistical methods for the analysis of repeated measurements, Springer, New York, 2002. https://link.springer.com/book/10.1007/b97287
4. A. W. Marshall, I. Olkin, A new method for adding a parameter to a family of distributions with application to the exponential and Weibull families, *Biometrika*, **84** (1997), 641–652. https://doi.org/10.1093/biomet/84.3.641
5. H. Lee, J. H. Cha, On two general classes of discrete bivariate distributions, *Am. Stat.*, **69** (2015), 221–230. https://doi.org/10.1080/00031305.2015.1044564
6. M. Goff, *Multivariate Discrete Phase-Type Distributions*, Ph.D. Thesis, Washington State University, 2001. Available from: https://hdl.handle.net/2376/303.
7. M. El-Dawoody, M. S. Eliwa, Bivariate discrete burr lifetime distribution: A mathematical and statistical framework for modeling medical and engineering data, *Inf. Sci. Lett.*, **12** (2023), 3199–3214. https://doi.org/10.18576/isl/121129
8. V. Nekoukhou, D. Kundu, Bivariate discrete generalized exponential distribution, *Statistics*, **51** (2017), 1143–1158. https://doi.org/10.1080/02331888.2017.1289534
9. D. Kundu, V. Nekoukhou, On bivariate discrete Weibull distribution, *Commun. Stat.- Theory Methods*, **48** (2019), 3464–3481. https://doi.org/10.1080/03610926.2018.1476712
10. M. S. Eliwa, M. El-Morshedy, Bayesian and non-Bayesian estimation of four–parameter of bivariate discrete inverse Weibull distribution with applications to model failure times, football, and biological data, *Filomat*, **34** (2020), 2511–2531. https://doi.org/10.2298/FIL2008511E
11. A. Barbiero, Discrete analogues of continuous bivariate probability distributions, *Ann. Oper. Res.*, **312** (2022), 23–43. https://doi.org/10.1007/s10479-019-03388-8
12. Y. M. Amer, D. Abdelhady, R. M. Shalabi, A novel family of continuous–discrete bivariate distributions, *Comput. J. Math. Stat. Sci.*, **5** (2026), 415–437. https://doi.org/10.21608/cjmss.2025.405765.1233
13. S. Kocherlakota, K. Kocherlakota, Bivariate discrete distributions, CRC Press, 2017. https://doi.org/10.1201/9781315138480
14. I. McHale, P. Scarf, Modelling soccer matches using bivariate discrete distributions with general dependence structure, *Stat. Neerl.*, **61** (2007), 432–445. https://doi.org/10.1111/j.1467-9574.2007.00368.x
15. H. Lee, J. H. Cha, New discrete bivariate distributions generated from discrete time point process model, *Methodol. Comput. Appl. Probab.*, **28** (2026), 41. https://doi.org/10.1007/s11009-026-10263-0

16. M. J. Lee, N. Y. Yoo, J. H. Cha, A new general class of discrete bivariate distributions constructed by the usual stochastic order, *Am. Stat.*, **79** (2025), 449–466. https://doi.org/10.1080/00031305.2025.2486306

17. J. Aitchison, C. H. Ho, The multivariate Poisson-log normal distribution, *Biometrika*, **76** (1989), 643–653. https://doi.org/10.1093/biomet/76.4.643

AIMS Press